Sun *et al. Energy Mater* 2024;4:400002
DOI: 10.20517/energymater.2023.63

Energy Materials

Review

Open Access

Constructing three-dimensional architectures to design advanced anodes materials for sodium-ion batteries: from nanoscale to microscale

Yu-Feng Sun[1], Yu Li[1,2,*], Yu-Teng Gong[1], Zhi-Xu Qiu[1], Ji Qian[1], Ying Bai[1], Zi-Lu Wang[1], Ri-Peng Zhang[1], Chuan Wu[1,2,*]

[1]School of Materials Science and Engineering, Beijing Key Laboratory of Environmental Science and Engineering, Beijing Institute of Technology, Beijing 100081, China.
[2]Yangtze Delta Region Academy of Beijing Institute of Technology, Jiaxing 314019, Zhejiang, China.

***Correspondence to:** Prof./Dr. Chuan Wu, School of Materials Science and Engineering, Beijing Institute of Technology, 5th Zhongguancun Street, Haidian District, Beijing 100081, China. E-mail: chuanwu@bit.edu.cn; Prof./Dr. Yu Li, School of Materials Science and Engineering, Beijing Institute of Technology, 5th Zhongguancun Street, Haidian District, Beijing 100081, China. E-mail: liyu0820@bit.edu.cn

How to cite this article: Sun YF, Li Y, Gong YT, Qiu ZX, Qian J, Bai Y, Wang ZL, Zhang RP, Wu C. Constructing three-dimensional architectures to design advanced anodes materials for sodium-ion batteries: from nanoscale to microscale. *Energy Mater* 2024;4:400002. https://dx.doi.org/10.20517/energymater.2023.63

Received: 27 Aug 2023 **First Decision:** 20 Sep 2023 **Revised:** 11 Oct 2023 **Accepted:** 14 Nov 2023 **Published:** 3 Jan 2024

Academic Editor: Xiongwei Wu **Copy Editor:** Fangling Lan **Production Editor:** Fangling Lan

Abstract

Sodium-ion batteries (SIBs) are emerging as a possible substitute for lithium-ion batteries (LIBs) in low-cost and large-scale electrochemical energy storage systems owing to the lack of lithium resources. The properties of SIBs are correlated to the electrode materials, while the performance of electrode materials is significantly affected by the morphologies. In recent years, several kinds of anode materials involving carbon-based anodes, titanium-based anodes, conversion anodes, alloy-based anodes, and organic anodes have been systematically researched to develop high-performance SIBs. Nanostructures have huge specific surface areas and short ion diffusion pathways. However, the excessive solid electrolyte interface film and worse thermodynamic stability hinder the application of nanomaterials in SIBs. Thus, the strategies for constructing three-dimensional (3D) architectures have been developed to compensate for the flaws of nanomaterials. This review summarizes recent achievements in 3D architectures, including hollow structures, core-shell structures, yolk-shell structures, porous structures, and self-assembled nano/micro-structures, and discusses the relationship between the 3D architectures and sodium storage properties. Notably, the intention of constructing 3D architectures is to improve materials performance by integrating the benefits of various structures and components. The development of 3D architecture construction strategies will be essential to future SIB applications.

Keywords: Sodium-ion batteries, anode materials, three-dimensional architectures, nanostructure, microstructure

INTRODUCTION

As the mainstay of contemporary industrialization, electricity boasts numerous applications, including heating, transportation, and telecommunication[1]. At present, most of the electricity is generated by the burning of nonrenewable fossil fuels, which raises problems with energy depletion and global warming[2-4]. Additionally, these questions lead to the redistribution of precipitation, the melting of glaciers and permafrost, and the rise in sea levels, which endangers human life and disturbs the ecosystem's delicate balance. In recent years, some renewable green power resources, including solar power and water power, have been used as supplementary or substitute resources for fossil energy[5]. However, limited by the natural environment, renewable energy sources have the characteristics of randomness, volatility, and instability. Once the electricity power is directly output, it can have a huge impact on the power grid, accompanied by large power loss. Thus, the expansion of sustainable energy technologies depends on the progress of large-scale energy storage systems[6]. Lithium-ion batteries (LIBs), a typical electrochemical storage system, have been widely applied in many types of portative electronics because of the less pollution and excellent energy density. However, the consumption of lithium resources is increasing, paralleled by the growing global demand for them. The rising price of lithium resources will prompt people to find new types of battery systems due to the unequal distribution of lithium sources in the crust of the Earth[7-9].

Compared to lithium, sodium is abundant and distributed across the Earth. Hence, extensive research has gradually shifted focus toward sodium-ion batteries (SIBs) since both sodium and lithium belong to an identical main group and have similar chemical and physical characteristics[10]. Although these two energy storage systems have parallel electrochemical reaction principles, the larger ionic radius of sodium (Li^+: 0.69 Å *vs.* Na^+: 0.98 Å) leads to lots of issues, including more serious volume variation and slower ion transfer and reaction kinetics[11]. Obviously, electrode materials that directly participate in electrochemical reactions could determine the performance of SIBs[12]. In the past few decades, some cathode materials, such as polyanionic compounds[13] and layered metal oxides[14], have been studied in depth and shown a high energy density, but the development of promising anodes seems to be in a relatively early stage. Accordingly, the progress of high energy density and excellent cycle stability anode materials is important to the future practical application of SIBs[15]. Five main categories of materials can be used as SIB anodes, which are carbon-based anodes, titanium-based anodes, conversion anodes, alloy-based anodes, and organic anodes. Various kinds of anode materials often exhibit distinct characteristics and properties. At present, the developed carbonaceous materials mainly include graphene, graphite sheets, carbon spheres, carbon fibers, carbon tubes, porous carbon, and amorphous carbon. Titanium-based anodes include titanium dioxide, spinel lithium titanate, and sodium titanate compounds. The conversion anodes mainly include different kinds of transition metal compounds, such as oxides, sulfides, selenides, and phosphides. Materials such as phosphorus, silicon, tin, antimony, and bismuth (Bi) belong to alloy-based anodes, and sodium is stored by alloying reaction between metals. In addition, some new organic materials can be used as anode materials, including carboxylate organics and polymers.

As is well known, the morphologies of materials should significantly affect their electrochemical performance because various microstructures show distinct surface and internal features. Due to the advancement of nanotechnology, nano-scaled materials in batteries have been massively fabricated to elevate the specific capacity and rate performance[16]. Nevertheless, nanomaterials have a higher specific surface area, making them more susceptible to side effects with electrolytes, leading to terrible electrochemical performance. While having shorter ion diffusion distances, nanomaterials also face worse thermodynamic stability, which will cause nanoparticles to agglomerate and battery life to be reduced. However, micro-materials with larger particle sizes exhibit inferior kinetics and lower energy density[17-19].

To deal with the constraints of nano- and micro-materials, the strategy of constructing three-dimensional (3D) architectures has been proposed[20]. Over the past few years, advances in 3D architecture construction have clearly demonstrated the indispensable position of this strategy in synthesizing and eventually optimizing battery materials[21-23]. Three-dimensional architectures are mainly composed of nanoscale building blocks (such as nanospheres, nanosheets, and nanoshells), which could reduce the ion/electron migration pathways and further return favorable kinetics and high capacities. Additionally, the 3D architectures can provide multiple transport channels, which will facilitate the transmission of electrons/ions[24]. Besides, the well-designed 3D electrode materials with excellent structural stability could also improve the cycling performance and increase volume energy density. As illustrated in Figure 1, 3D architectures can be classified into five types, depending on their morphological characteristics: hollow structures, core-shell structures, yolk-shell structures, porous structures, and self-assembled nano/micro-structures. Hollow structures have a large specific surface area and great deformation resistance, which can improve rate performance and cycle life[25-27]. Core-shell structures are constructed by tightly combined shell and core, whereas yolk-shell structures are made up of separated core and shell. They offer distinct advantages in terms of enhancing anode material electrochemical performance. Core-shell structures have a high volume energy density and rich heterogeneous interface, while yolk-shell structures reduce volume expansion during charge and discharge[28-30]. Hollow, core-shell, and yolk-shell structures can be further classified into single, multi-core/shell, and hierarchical structures, which have different construction strategies and unique performance advantages. Besides, porous structures, which can be categorized into microporous, mesoporous, and macroporous structures according to the pore size, provide a large number of sodium storage sites and ultrafast sodium ion pathways[31,32]. Self-assembled nano/micro-structures are a combination of nanostructures and microstructures. Assembling nanostructures into microstructures can improve the ion/electron exchangeability and structural stability of anode materials. Generally, self-assembled nano/micro-structures include thousands of morphological features that can typically be classified into two types by different self-assembly ways: (i) several nanostructures self-assemble to create microstructures; and (ii) nanostructures are embedded within another structure to form microstructures[19,33,34].

In this review, we attempt to comprehensively summarize the latest progress in 3D architectures in anode materials for SIBs. We describe the definition, advantages, and disadvantages of 3D architectures, including hollow structures, core-shell structures, yolk-shell structures, porous structures, and self-assembled nano/micro-structures. Additionally, the design thought, synthesis method, electrochemical performance, and sodium storage mechanism of each unique morphology are summarized by a detailed analysis of several examples. Prior to this, we briefly introduce the typical SIB anode families, including carbon-based anodes, titanium-based anodes, conversion anodes, alloy-based anodes, and organic anodes, so we can comprehend the advantages of each type of anode material and the dilemma they suffered.

TYPICAL FAMILIES OF ANODES FOR SIBS

Carbon-based anodes

Based on the reversible deintercalation reaction of lithium ions, graphite materials have been successfully applied to the anode for LIBs. In fact, carbon-based anode materials have long played a vital role in electrochemical energy storage (EES), so researchers pay special attention to the application of carbon-based anodes for SIBs[35]. Although sodium ions have similar chemical properties to lithium ions, graphite and sodium cannot form thermodynamically stable compounds in traditional ester-based electrolytes, leading to the fact that commercial graphite anodes cannot be used as anodes for SIBs[36]. At present, the developed carbonaceous materials mainly include graphene, graphite sheets, carbon spheres, carbon fibers, carbon tubes, porous carbon, and amorphous carbon. Generally, the specific capacity of carbon-based anodes is 200~500 mAh g^{-1}[37]. Additionally, because of the advantages such as a wide range of sources, non-toxicity, air stability, and low cost, carbon-based materials are considered as suitable anodes for SIBs. Generally, the

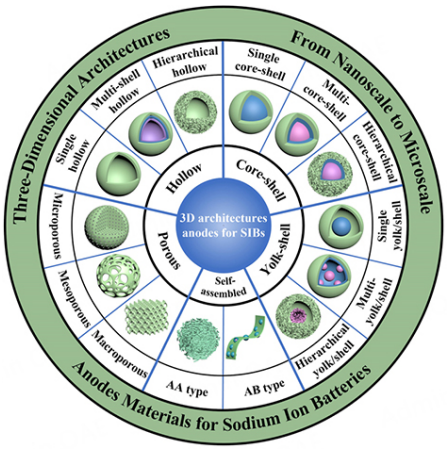

Figure 1. Different types of three-dimensional architectures of anode materials for SIBs.

widely studied carbon-based anodes for SIBs can be divided into four categories: graphite, graphene, hard carbon, and soft carbon materials[38].

Graphite and graphene are typical two-dimensional (2D) layered materials. Graphite, which is a widely used anode in LIBs, offers an excellent specific capacity (372 mAh g^{-1}), but its performance in SIBs is not satisfactory. In 1988, Ge *et al.* found that graphite would form NaC_{64} compounds with sodium, and the specific capacity of sodium storage was only 35 mAh g^{-1}[39]. Therefore, over the past few decades, researchers determined that graphite was not suitable for SIB anodes. Until 2014, when Jache *et al.* applied ether electrolytes in SIBs, graphite anodes showed excellent sodium storage performance, attracting significant attention from numerous researchers[40]. In particular, hard carbon is characterized by its resistance to graphitization above 2,500 °C, making it a crucial material in the development of SIBs. Dahn first introduced glucose-based hard carbon as anode materials into SIBs and found that hard carbon had a high specific capacity (300 mAh g^{-1}) and an ideal sodium storage platform (~0.1 V)[41]. This discovery has aroused widespread research interest. In the next 20 years, a variety of biomass precursors have been used to prepare hard carbon, such as grapefruit peel, peat moss, banana peel, seaweed, ramie, and natural polymer phenolic resin[42-45]. Soft carbon is a unique type of carbon material that has disordered nanostructures and ordered carbon layers. Heat treatment can change the degree of graphitization of soft carbon. Different from hard carbon, it will transform into graphite when heated above 2,500 °C. The carbon layer of soft carbon is more ordered and longer, and the conductivity is higher, resulting in a relatively good rate performance. Besides, the low defect concentration and small specific surface area of soft carbon could weaken the decomposition degree of electrolytes and help to improve the Coulombic efficiency of the first cycle. It is worth noting that the voltage range of soft carbon sodium storage usually falls between 0.2 and 1.2 V, higher than the voltage of sodium deposition, contributing to improved safety. However, a high voltage range will reduce the voltage window of the whole battery, which is not conducive to the energy density of the cell. In terms of synthetic precursors, soft carbon can usually be prepared by conversion of polypyrrole (PPy), asphalt, tar, and hydrocarbon-based materials. From a practical point of view, soft carbon has the potential for practical applications due to its low price, high carbon production rate, excellent safety, and good sodium storage performance.

Titanium-based anodes

Although the comprehensive performance of hard carbon is quite eminent, the capacity contribution potential of hard carbon materials is mainly at 0~0.1 V, which is close to the sodium plating potential. Therefore, there is a risk of sodium precipitation that leads to safety problems[46]. In SIBs, the redox potential of Ti^{3+}/Ti^{4+} is usually between 0.5 and 1.0 V, which effectively avoids the dangerous sodium deposition behavior and ensures strong stability during large-scale energy storage. In addition, titanium-based anodes

can provide long cycle life in SIBs due to their low lattice stress. Therefore, titanium-based anodes are regarded as potential substitutes for SIBs, which can embed/remove sodium ions reversibly while maintaining structural integrity. During the past few decades, many different kinds of titanium-based compounds, such as titanium dioxide, spinel lithium titanate, and sodium titanate, have drawn the interest of scientists in the light of the obvious benefits of titanium-based compounds: inexpensive, nontoxic, appropriate working voltage, small strain, and excellent cycle stability[47]. At present, most of the research on titanium-based compounds focuses on optimizing electrochemical performance and exploring electrochemical mechanism[48].

Conversion anodes

Binary metal compounds, which can store sodium ions through the conversion reaction mechanism, are expected to become the alternative anodes for SIBs owing to the great abundant species and excellent theoretical specific capacity[49]. Nevertheless, binary metal compounds in the conversion reaction mechanism usually face problems such as poor reversibility, significant voltage hysteresis, severe volume expansion, and poor initial Coulombic efficiency (ICE) and cycle performance. To overcome these challenges, several new strategies have been proposed, including material structure design, nanocrystallization, surface engineering, and electrolyte optimization[50]. The following reaction equation can be used to represent the conversion reaction between binary metal compounds and sodium:

$$M_aX_b + (b \cdot z)Na \leftrightarrow aM + bNa_zX \quad (1)$$

In general, M can be one of the transition metal elements, mainly including Fe, Mn, Ni, and so on. On the contrary, X is one of the nonmetallic elements, including O, S, Se, P, and so on. For some special conversion anodes, the conversion reaction and alloying reaction will both occur during the sodium storage process. This occurs because some M elements will continue to react with sodium to form alloys, indicating that the capacity contribution is derived from two aspects of alloying and conversion reaction mechanism. Therefore, M_aX_b anodes often have a larger theoretical specific capacity than pure M metal anodes[51]. Besides, the conversion anodes usually transform into nanoparticles via phase separation during charge and discharge. In theory, nanoparticles have a higher specific surface area and shorter ion diffusion distances, which facilitates the reversibility of e^-/Na^+ transmission and conversion reactions. The interface of the electronic conductive phase (M) and ionic conductive phase (Na_zX) can store more Na^+ through the "sharing" mechanism to generate additional capacity[52]. However, a larger specific surface area means that nanoparticles are more susceptible to side effects with electrolytes, leading to terrible electrochemical performance. Besides, the crushed anode particles are more prone to fall off from the electrode, resulting in battery failure.

Conversion anodes, depending on their thermodynamic properties, can be employed as both positive and negative electrodes in batteries[53]. Although the conversion reaction can be carried out through the intermediate phase, which determines the actual voltage capacity curve, it has little influence on the theoretical specific capacity and average potential. Besides, thermodynamic data can be used to contrast the main characteristics and distinctions of Li and Na conversion reactions. By using the Gibbs free energy of the conversion reaction (ΔrG), Klein *et al.* revealed the potential difference of the conversion reaction between M_aX_b and Li or Na[54]. Compared with the conversion anodes of LIBs, M_aH_b, M_aO_b, M_aS_b, and M_aF_b for SIBs show lower redox potentials, while M_aBr_b and M_aI_b provide higher redox potentials.

Alloy-based anodes

The main group elements of IV and V (P, Si, Bi, Sn, Sb, Ge, *etc.*) can form binary alloys to store sodium by alloying with Na^+, providing high sodium storage capacity, which can serve as an anode for the development

of high-capacity SIBs[55]. Different from the reversible intercalation-deintercalation mechanism of carbon and titanium-based anode materials, alloying reaction anode materials are carried out through a series of chemical bond formation or fracture and structural evolution. The sodium reaction of alloyed anode materials occurs at low potential, which can produce high energy density[56]. Alloying reactions can usually be expressed as:

$$M + xNa^+ + xe^- \leftrightarrow Na_xM \quad (2)$$

Many alloy anode materials may have multiple intermediate phases before the alloying reaction reaches the final state. Although the phase diagram can be used to predict the intermediates formed in the sodiation/desodiation process, there are still some situations where the experimental results do not match the theoretical predictions. The resulting alloying products determine the volume change and the specific capacity. Therefore, the alloying reaction mechanism still needs further study.

The anodes based on alloying reactions have excellent specific capacity and rate performance. Among them, the black phosphorus exhibits an outstanding sodium storage capacity (> 2,000 mAh g^{-1}), which is considered to be highly suitable for the development of anodes for high-capacity SIBs. Although significant research improvement has been made in alloy-based anodes during the past few years, and numerous alloy-based anodes with high capacity have been developed, the alloy reaction usually causes huge volume changes, resulting in the pulverization of active substances. In addition, the stress and strain generated by the huge volume change have a chain reaction, which will cause a series of adverse effects. For example, the unstable solid electrolyte interface (SEI) film, the shedding of active substances from the collector, and the large voltage lag caused by deformation will aggravate the decline of electrode performance. Sn[57], Ge[58], Sb[59], and Bi[60] exhibit great rate performance despite having low specific capacities due to their excellent electronic conductivity. Although P[61] and Si[62] have high theoretical specific capacity, their poor electrical conductivity leads to slow reaction kinetics. Some common methods can improve the defects of alloy anodes to some extent, such as material nanocrystallization, surface coating, building composite electrodes, and optimizing binders and electrolytes[63]. At present, alloying anode materials remain on the laboratory scale, and there is no successful case of mass production, especially nanostructured alloy anode materials, so more efforts are still needed to make alloying anode materials practical.

Organic anode materials

Due to the sodium storage mechanism of multi-electron reversible redox reactions, organic electrode materials have abundant natural resources, diverse structures, and high electrochemical performance, which provide a possible choice for the design of green SIBs with high capacity, low cost, sustainability, and flexibility. The application of organic electrodes in SIBs is not a new technology. As early as the 1980s, studies have explored the possibility of inserting Na^+ into organic electrodes. After that, polyacetylene and polyphenylene oxides have been successfully used as polymer-based anodes for non-aqueous rechargeable batteries, such as SIBs, according to Shacklette[64]. During the past few years, many research groups have begun to conduct in-depth studies on organic compounds to explore their potential sodium storage characteristics. At present, it is found that organic materials that can be used as anodes of SIBs should be roughly divided into two categories: polymers and organic small molecules. Among them, Schiff base polymers, polyquinones/polyamides and conductive polymers are several typical kinds of polymers for SIBs anodes[65].

According to species and sodium storage mechanism, the anode materials of SIBs may generally be categorized into five types. Among them, carbon-based anodes and titanium-based anodes store sodium

through an insertion reaction. The carbon-based anode has been widely used in commercial SIBs due to their abundant raw material sources and low cost. Ti-based anodes have excellent structural stability but also suffer high operating voltage and low theoretical specific capacity. Alloy-based anodes store sodium by alloying reactions, which can form a binary alloy between metal and sodium. The sodium storage mechanism of conversion anodes is the conversion reaction, which is similar to the substitution reaction. In fact, both alloy anodes and conversion anodes could provide ultra-high theoretical specific capacity. However, their challenge lies in poor cycle stability due to the severe volume expansion during sodium storage. Organic anodes can store sodium through multi-electron redox reactions, but the poor conductivity of organic materials and the solubility of organic molecules in electrolytes hinder the development of organic anodes.

STRATEGIES FOR CONSTRUCTING 3D ARCHITECTURES

Hollow structure

Hollow structures are one of the most common 3D architectures, which are widely used in the EES field. Generally, an architecture containing a shell and a cavity can be defined as a hollow structure. However, to summarize the application of hollow anodes in SIBs, we classify and define three kinds of hollow structures to distinguish them from other complex 3D architectures. Hollow anodes can be divided into single hollow structures, double/multilayer hollow structures, and hierarchical hollow structures. In fact, these hollow structures have long been studied in LIBs[24]. As a potential substitute for LIBs, SIBs have similar research ideas, including material selection and structure design. However, the SIB anode faces a more serious volume expansion problem, which means that the structure of the anode material is more likely to collapse and lead to failure. At the same time, the reaction kinetics of sodium ions are slower because of their larger ionic radius. Therefore, more attention needs to be paid to the 3D architecture construction from the nanoscale to the microscale while designing hollow structures. Here, we summarize the research results of these structures for SIBs in recent years.

Single hollow structure

Single hollow structures consist solely of a single shell and a cavity. Moreover, the shell of single hollow structures is uniformly constructed by nanoparticles or rolled by 2D layered materials, and there are no more complex building blocks. Single hollow structures mainly include hollow spheres and hollow tubes. Among these, carbon-based anode materials are the most studied materials with hollow sphere structures. In fact, hollow carbon materials are an important member of the carbon material families and are generally used in EES fields, such as supercapacitors, SIBs, and lithium sulfur (S) batteries. With the general advantages of hollow structural materials, they also have low specific density, good mechanical strength, and excellent thermal stability. Tang *et al.* reported hollow carbon nanospheres applied to the anodes of SIBs for the first time[66]. They designed a simple hydrothermal carbonization approach to prepare hollow carbon spheres by using latex as the template and obtained hollow carbon nanospheres after removing the template. The thickness of a carbon shell is about 12 nm, mainly composed of disordered graphite-like structures. At 50 mA g^{-1}, the initial discharge capacity of prepared hollow carbon nanospheres is up to 537 mAh g^{-1}, followed by a reversible capacity of about 200 mAh g^{-1} [Figure 2A-C]. Compared with the anodes of SIBs at that time, this is already a considerable reversible capacity. In addition, they studied the rate performance difference between hollow nanospheres and solid nanospheres, and the results showed that hollow nanospheres always had a higher reversible capacity [Figure 2D and E]. It has been proved that the unique hollow carbon structure has excellent reversible capacity and rate capability due to its large electrolyte/electrode contact area and thin shell thickness. In recent years, hard carbon has grown to be the most widely used anode for SIBs due to its ideal sodium storage platform (~0.1 V) and high specific capacity[67]. To further improve its electrochemical performance, Chen *et al.* obtained hollow hard carbon nanospheres via pyrolysis of phenolic resin using SiO_2 as a template[68]. As shown in Figure 2F-H, hollow

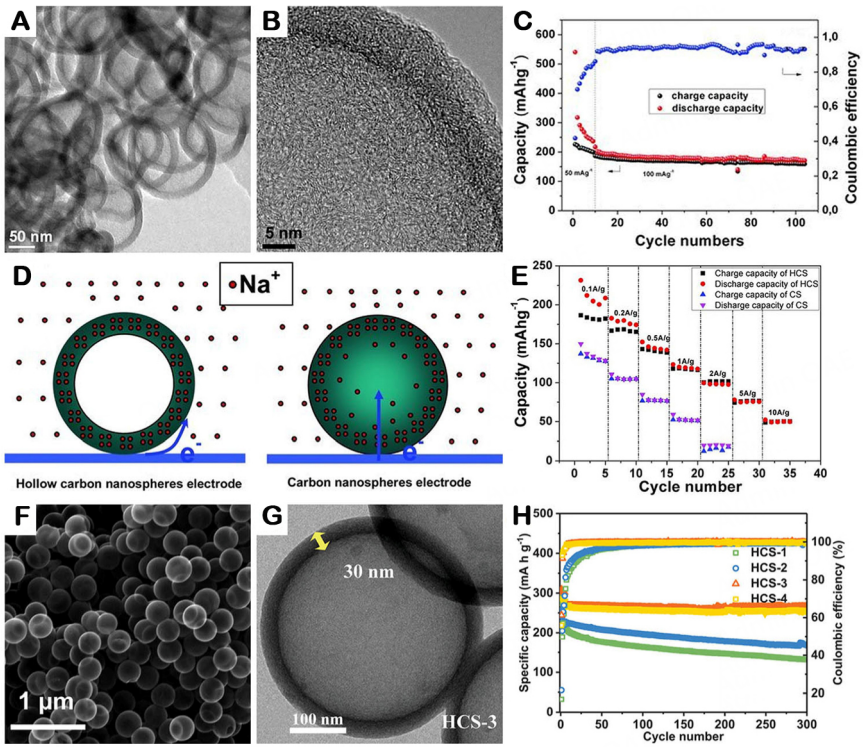

Figure 2. (A) TEM, (B) HR-TEM images, and (C) cycling performance of hollow carbon nanospheres. (D) Schemes of the electrochemical reaction process and (E) rate performance of hollow carbon nanospheres and carbon nanospheres electrode[66]. (F) SEM and (G) TEM images and (H) cycling performance of hollow carbon spheres[68].

hard carbon nanospheres with a 30 nm shell showed the most ideal electrochemical performance. The reversible capacity is 266.2 mAh g^{-1} after 300 cycles, and the capacity retention rate is up to 98.1%. This study showed that the behavior of hollow hard carbon nanospheres conformed to the "adsorption-intercalation" mechanism. With the increase of carbon layer thickness, the low-potential plateau (LPP) capacity of hard carbon gradually increased, and the high-potential sloping (HPS) capacity gradually decreased.

Comparable to hollow spheres, hollow tubes are also a kind of common hollow structure. Usually, the size of hollow tubes in one direction is much larger than in other directions. Hollow tubes have good buffer capacity to effectively resist the volume expansion of anodes during sodiation. Additionally, the winding among hollow tubes can build a large conductive framework, connecting with each other to provide a good electronic transmission path. Han *et al.* used the electrospinning method to synthesize hollow carbon nanofibers (HCNFs), and PMMA is the template [Figure 3A][69]. The carbon nanofibers (CNFs) have a length of tens of microns, a diameter of about 1 μm, a wall thickness of about 130 nm, and a low Brunauer-Emmett-Teller surface area of 21.8 m^2 g^{-1}. Compared with ordinary CNFs, hollow nanofibers have higher charge capacity (326 mAh g^{-1}) and higher ICE (70.4%). In the rate test, the reversible capacity of HCNFs at different current densities is higher than that of ordinary CNFs. After 450 cycles, the capacity retention of common carbon nanotubes decreased to 35.5%, while the HCNFs reached 70% after 5,000 cycles at 1.6 A g^{-1} [Figure 3B-D]. These excellent performance outcomes benefit from larger inner diameters, appropriate wall thicknesses, and interconnected 3D frameworks. To significantly enhance the performance of hollow carbon nanotubes, Zhong *et al.* reported a high-performance nitrogen (N)-rich hollow carbon nanotubes (NCNTs) for LIBs and SIBs [Figure 3E and F][70]. The nitrogen content reached 15.7%, and the aspect ratio

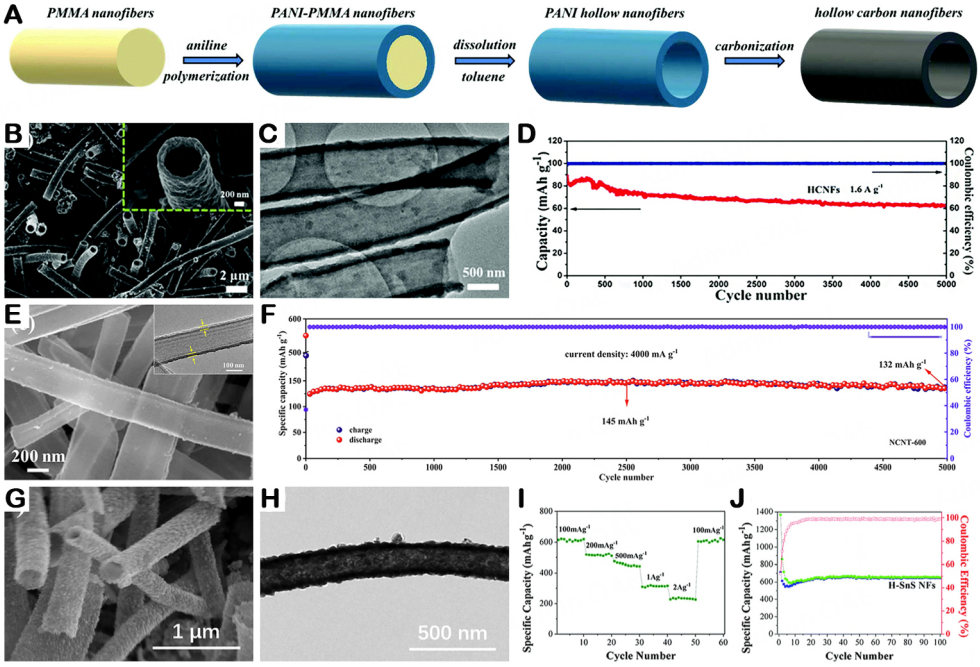

Figure 3. (A) Schematic of the synthesis, (B) SEM and (C) TEM images, and (D) cycling performance of hollow carbon nanofibers (HCNF)[69]. (E) SEM and TEM images, (F) cycling performance of nitrogen-rich hollow carbon nanotubes (NCNT)[70]. (G) SEM and (H) TEM images, (I) rate performance, and (J) cycling performance of SnS hollow nanofibers (SnS HNFs)[71].

was 12 μm/200 nm. NCNTs showed excellent reversible capacity, maintaining 198 mAh g^{-1} after 3,000 cycles at 1 A g^{-1}. Meanwhile, they also have reliable cycling performance and enhanced rate performance (132 mAh g^{-1} after 5,000 cycles at 4 A g^{-1}). This study suggests that N doping brings more active sites and defects, resulting in the improvement of electrochemical performance. Apart from carbon-based anodes, some conversion anodes also have strategies to construct hollow structures. Conversion anodes usually have higher specific capacity and poor cycling capacity than carbon-based anodes because they tend to have more serious bulk expansion. Therefore, reasonable construction of microstructures is an important strategy to enhance the electrochemical properties of the conversion anodes. For example, Jia *et al.* developed a SnS hollow nanofibers (SnS HNFs) for high-performance SIBs [Figure 3G-J][71]. SnS HNFs maintained a specific capacity of 645 mAh g^{-1} after 100 cycles at 0.1 A g^{-1} and 310 mAh g^{-1} at 1 A g^{-1}. For the conversion anode, a larger specific surface area favors redox reactions, while thinner walls favor ion diffusion. This strategy of constructing hollow structures could be implemented in other conversion anodes.

The above studies have shown that the anode materials with hollow structures often show better electrochemical performance than the solid materials, which is due to the low BET surface area, thin shell, and open interior. However, single hollow structures also have many limitations. Researchers should develop many complex hollow structures in continuous exploration, which can often provide better electrochemical performance.

Double/multi-shell hollow structure

A double-layer hollow structure consists of two layers of shells and cavities, usually comprising distinct materials or phases in each of the shell layers. Carbon layers usually play an important role in double-layer hollow structures. Thin carbon coating can limit the inner material, which will effectively resist the volume expansion during sodiation. Meanwhile, the carbon layer can also increase the conductivity. Hou *et al.*

prepared a double-layer $NaTi_2(PO_4)_3$@C hollow nanocubes (NTP@C) for aqueous SIBs by hydrothermal methods[72]. As shown in Figure 4A-D, NTP@C is composed of an inner layer of 15 nm ($NaTi_2(PO_4)_3$) and an outer layer of 5 nm (carbon layer). The NTP@C//$Na_{0.44}MnO_2$ aqueous SIB assembled with deep eutectic electrolytes showed an ultra-high energy density (50.0 Wh kg^{-1}, according to the overall cathode and anode weight) and ultra-long cycle life (3,500 cycles, capacity retention rate of 90%). Benefiting from the carefully designed negative structure, this battery will hopefully become a candidate for large-scale energy storage. Zhang *et al.* synthesized a double-layer ZnS-SnS@C hollow nanobox (H-ZSS@C@G) for LIB and SIB anodes and used graphene for encapsulation [Figure 4E-H][73]. The outer layer of the nanobox is a carbon layer, and the inner layer is composed of ZnS-SnS heterostructures. At 10 A g^{-1}, H-ZSS@C@G still has a reversible capacity of 347 mAh g^{-1} and excellent cycling performance (247 mAh g^{-1} after 1,000 cycles at 2 A g^{-1}).

Similar to the single hollow structure, the double-layer hollow tube is also a typical double-layer hollow structure. Liu *et al.* designed a coaxial double hollow nanotube structure [Figure 4I-L][74]. This kind of nanotube is formed by coating the carbon layer evenly on the Sb hollow tube, and the hollow structure can be changed by adjusting the annealing time. Sb is a type of high theoretical capacity anode (660 mAh g^{-1}), but it will lead to rapid capacity attenuation due to the volume change during sodiation and desodiation. The results showed that the coaxial double-layer hollow structure greatly improves the rate and cycling performance of Sb, which has the following reasons: (i) The large cavity in the nanotubes allows the Sb nanotubes to expand; and (ii) The coated carbon layer prevented the formation of unstable SEI film by isolating Sb from the electrolyte.

A multilayer hollow structure is mainly composed of three or more shells and cavities. Bin *et al.* constructed multi-shell hollow carbon nanospheres (MS-HCNs), each layer of which is carbon material[75]. By controlling the polymerization process of 3-aminophenol (3-AP)/formaldehyde (3-AF) resin, they realized the accurate regulation of the shell number of hollow nanospheres [Figure 5A and B]. Studies have shown that the reversible capacity of MS-HCNs is enhanced as the shell number increases. Among them, the four-layer shell HCNs have the best reversible capacity (360 mAh g^{-1} at 30 mA g^{-1}) and excellent rate performance [Figure 5C and D]. Wang *et al.* prepared two-to-five-shell cobalt sulfide hollow nanoboxes by an "ion conversion and exchange" strategy based on metal-organic frameworks (MOF), as shown in Figure 5E-G[76]. By adjusting the temperature, the number of shells can be easily controlled. Among them, the three-shell nanobox can provide an excellent specific capacity of 438 mAh g^{-1} after 100 cycles at 500 mA g^{-1}. In these multi-shell nanoboxes, the voids between different shells provide sufficient space to resist volume expansion, and the authors believe that the large cavity and thin shell also contribute to excellent performance.

Hierarchical hollow structure

Hierarchical hollow structure is usually composed of complex nanostructure, among which hollow nanospheres composed of 2D layered nanosheets are more common. This structure presents a hollow structure at the micron scale and is composed of many nanosheets at the nanoscale. As a piece of evidence, Yang *et al.* reported a hierarchical hollow structured vanadium tetrasulfide (VS_4) for SIBs [Figure 6A-D][77]. The shell of hollow VS_4 microspheres is composed of numerous ultrathin nanosheets, which can reduce the stress caused by volume expansion [Figure 6E and F]. The reversible capacity is about 378 mA hg^{-1} at 10 A g^{-1}, while the capacity retention is 73.2% after 1,000 cycles [Figure 6G]. In addition, the hollow VS_4 microspheres have good low-temperature performance and exhibit good rate performance at -40 °C. This study showed that the combination of 2D nanosheets and hollow structures can effectively improve the electrochemical properties of VS_4, owing to the rapid reaction kinetics of nanosheets and the stress buffer

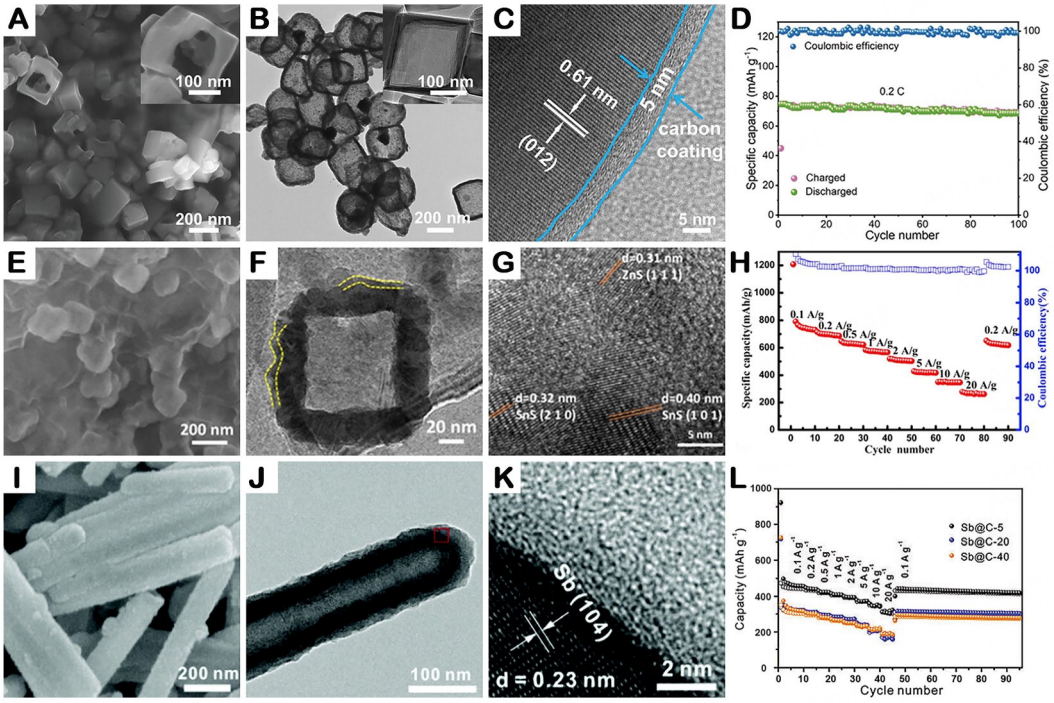

Figure 4. (A) SEM, (B) TEM, and (C) HR-TEM images and (D) cycling performance of $NaTi_2(PO_4)_3$@C hollow nanocubes (NTP@C)[72]. (E) SEM, (F) TEM, and (G) HR-TEM images and (H) rate performance of ZnS-SnS@C hollow nanobox [(H)-ZSS@C@G][73]. (I) SEM, (J) TEM, and (K) HR-TEM images and (L) rate performance of Sb@C coaxial hollow nanotubes[74].

capacity of hollow structures. Xie *et al.* assembled N-doped carbon-coated ultrathin nanosheets into homogeneous $Na_2Ti_3O_7$ hollow spheres [Figure 6H-J][78]. As shown in Figure 6K, the $Na_2Ti_3O_7$ hollow sphere can provide enhanced reversible capacity (≈60 mAh g^{-1}) at 50 C, which is much higher than the material assembled bare nanosheets, indicating the superiority of the hierarchical structure. Ru *et al.* proposed a new covalent assembly approach for MoS_2 nanosheets. By using SnS nanoparticles as covalent bridges, the MoS_2/SnS hollow superassemblies (HSs) have been prepared [Figure 6L and M][79]. HSs exhibit excellent rate performance when applied in SIBs. At 10 A g^{-1}, they had a reversible capacity of 368 mAh g^{-1}. The capacity retention rate reached 90.61% after 150 cycles at 0.5 A g^{-1} [Figure 6N].

Core-shell structure

The core-shell structure is a 3D architecture consisting of several shells and cores, and there is almost no void between the core and shell. Compared with hollow structures, core-shell structures usually have good resistance to volume expansion. During charge and discharge, the core and shell support each other and limit volume changes to each other. In addition, since there is no cavity, the core-shell structure usually has a larger density than the hollow structure, which also means higher volume capacity. There are three typical kinds of core-shell structure:

Single Core/shell structure

A single core-shell structure usually consists of a shell and a core. This structure can maintain a stable microstructure while having both core and shell electrochemical properties. As common coatings, carbon materials also play an important role in forming core-shell structures. The research showed that[80] carbon-based core-shell structures have a series of advantages, and one of the most beneficial approaches to enhance the synergistic effect and reaction kinetics is to build core-shell structures: (i) For the shell, carbon

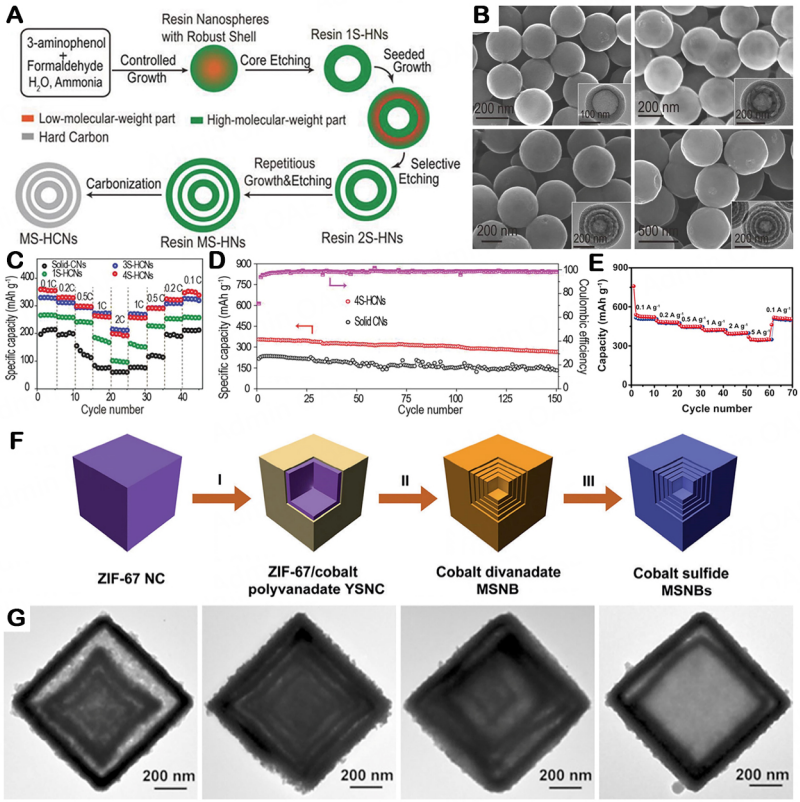

Figure 5. (A) Schematic of the synthesis, (B) SEM and TEM images, (C) rate performance, and (D) cycling performance of multi-shell hollow carbon nanospheres (MS-HCNs)[75]. (E) rate performance, (F) schematic of the synthesis, and (G) TEM images of two-to-five-shell cobalt sulfide hollow nanoboxes[76].

is a suitable choice to achieve fast electron and ion transfer; (ii) Core-shell structures can significantly reduce the distance of ion diffusion and provide rich active sites; (iii) Synergy between shells and cores results in excellent durability for long cycle performance; and (iv) Rich heterogeneous interfaces result in lattice defects and mismatches, which are needed to increase the active sites, specific surface area, and porosity. Osman *et al.* designed a simple one-pot approach to produce core-shell V_2O_5@C for symmetric batteries (used as both positive and negative electrode materials)[80]. Amorphous V_2O_5 has great theoretical specific capacity but only provides poor mechanical strength and conductivity. However, the amorphous V_2O_5 with carbon-coated core-shell structures exhibits excellent rate performance and cycling ability. As shown in Figure 7A-C, the thickness of a carbon shell is about 35 nm. As an anode material, it offers an initial capacity of 435 mA g^{-1} at 50 mA g^{-1} and retains 95% capacity after 3,000 cycles at 2 A g^{-1}. The fully symmetrical battery assembled by V_2O_5@C provides a long cycle life of over 1,000 cycles and an energy density of 381 Wh kg^{-1} at 1.0 A g^{-1} [Figure 7D]. Recently, transition metal sulfides gained great popularity as the candidate of SIB anodes, which benefit from their excellent electrochemical activity and high theoretical capacity, but they also face serious volume expansion and poor cycle stability[81]. Constructing a stable core-shell structure is one of the efficient solutions to resist the volume expansion. Zhu *et al.* reported a carbon-coated manganese sulfide nanocube with a core-shell structure[82]. Under the coating of carbon, the volume expansion and low conductivity of MnS are well improved. At the same time, the simultaneous doping of N and S in the carbon (NSC) shell effectively solves the dissolution of the polysulfide intermediate produced by MnS during charge and discharge. Figure 7E-G shows that the diameter of the MnS cube is about 50~100 nm, and the carbon shell is about 10 nm. MnS@NSC delivers a reversible capacity of 594.2 mAh g^{-1} at 0.1 A g^{-1}, far exceeding that of individual MnS and NSC materials. In the long cycle test, the reversible capacity of

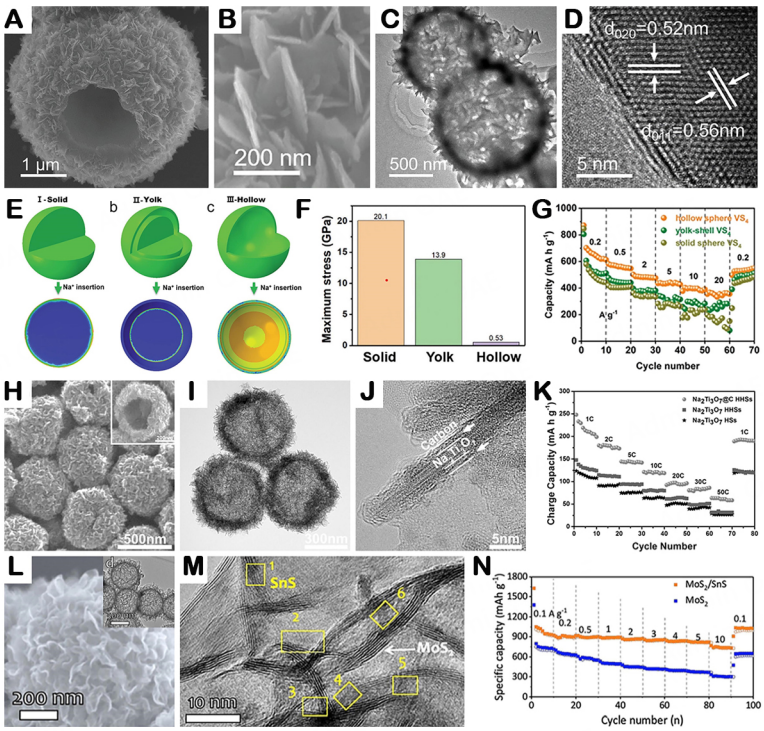

Figure 6. (A and B) SEM, (C) TEM, and (D) HR-TEM images of VS_4 hierarchical hollow spheres, (E) FE models and (F) the maximum stress of three different structures, (G) rate performance of VS_4[77]. (H) SEM, (I) TEM, and (J) HR-TEM images and (K) rate performance of $Na_2Ti_3O_7$ hollow spheres[78]. (L) SEM and (M) HR-TEM images and (N) rate performance of MoS_2/SnS hollow superassemblies (HSs)[79].

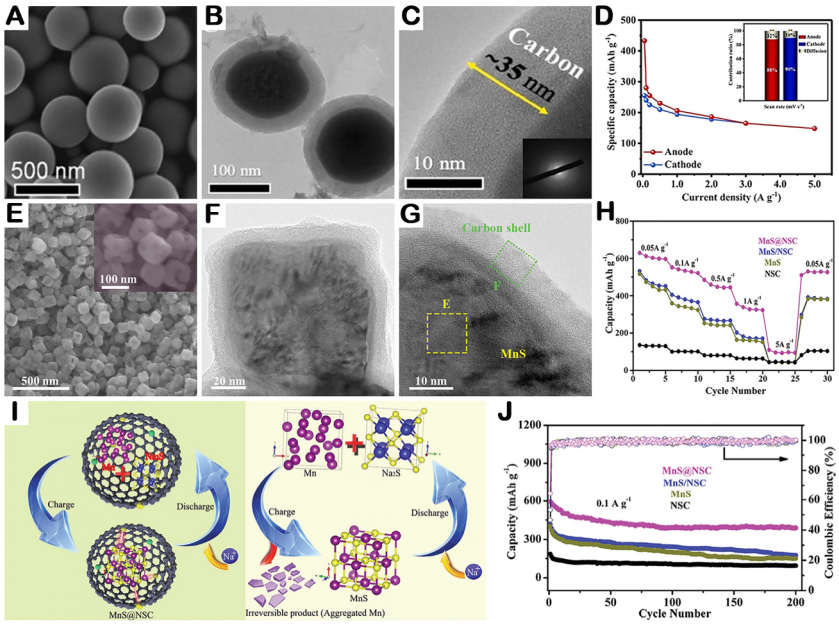

Figure 7. (A) SEM, (B) TEM, and (C) HR-TEM images and (D) rate performance of core-shell V_2O_5@C[80]. (E) SEM, (F) TEM, and (G) HR-TEM images and (H) rate performance of carbon-coated MnS (MnS@NSC). (I) Schematics comparing the sodiation/desodiation process in core-shell MnS@NSC and bare MnS, (J) cycling performance of MnS@NSC[82].

MnS@NSC retains 79.5% after 3,000 cycles at the current density of 1 A g^{-1} [Figure 7H-J]. The authors believe that the excellent performance of MnS@NSC with core-shell structures mainly comes from the following reasons: (i) The limiting effect of carbon shells on MnS effectively reduces the volume expansion of MnS without affecting ion transport; and (ii) A strong C-S-MnS bond forms between manganese sulfide and carbon as a result of N and S co-doping, which effectively prevents the aggregation of Mn particles and helps MnS achieve Na storage.

Lim *et al.* reported a core-shell MoS_2/silicon carbide (SiOC) anode material[83]. As shown in Figure 8A-C, a SiOC coating (~10 nm) is homogeneously coated on the MoS_2 sphere, forming a typical core-shell structure. In the experiment, the N-MoS_2/C@SiOC anode showed much higher reversible capacity, cycling ability, and rate performance than other MoS_2-based anodes [Figure 8D]. The capacity retention is 128% after 200 cycles at 0.1 A g^{-1}. Studies have shown that the SiOC shell successfully inhibits the volume expansion of MoS_2 and keeps its effect during the long cycle. In addition, SiOC acts as a channel between the core and the shell, which enables rapid ion and electron exchange and prevents excessive contact between the electrolyte and the core. As mentioned above, one of the advantages of core-shell structures is their higher density. Tellurium-based materials are typical high-density anode materials widely used in LIBs and SIBs. Zhang *et al.* designed a core-shell ZnTe@N-doped carbon nanowire with high weight and volume capacity[84]. It can be seen from Figure 8E-G that the prepared ZnTe@C nanowires are composed of carbon shells and ZnTe cores, which is a typical single core-shell structure. Their average diameter is about 62.3 nm, and the shell thickness is about 15 nm. ZnTe@C nanowires exhibit enhanced performance in both SIBs and LIBs. After 100 cycles at 50 mA g^{-1}, ZnTe@C offers a capacity of more than 400 mAh g^{-1}. Compared with the ordinary ZnTe electrode, the initial capacity of ZnTe@C nanowires is not much different, but they have better rates and cycling performance, which is attributed to the compact core-shell structure [Figure 8H]. Introducing conductive carriers or skeletons is one of the effective solutions to solve the problem of poor cycling performance of mesoporous biological carbon materials as SIB anodes. Titanium carbide (TiC) has become an ideal electrochemical carrier material due to its good electrical conductivity and chemical stability. Shen *et al.* reported a core-shell TiC/C anode material for SIBs [Figure 8I-L][85]. In fact, TiC does not function directly as an active material but rather as a skeleton for carbon materials; the core-shell TiC/C nanowires exhibit enhanced cycling performance and reversibility compared with other carbon anodes. After 300 cycles at 200 mA g^{-1}, they retain 89.15% capacity (90.14% after 1,000 cycles at 2 A g^{-1}). The excellent performance of TiC/C is due to its core-shell structure, which combines the high stability of the core (TiC) and the electrochemical properties of carbon shells.

Multi-core/shell structure

Multi-core/shell structures consist of multilayer shells or multiple cores, usually with more complex 3D configurations such as multi-shell or multi-core. Liu *et al.* synthesized a multilayer core-shell Sn nanorod for SIBs using a tobacco mosaic virus (TMV) as a biological template [Figure 9A-C][86]. As one of the alloy-based anodes, Sn offers an ultra-high theoretical specific capacity (847 mAh g^{-1}). Nevertheless, the volume change of Sn during the alloying process is large, and the material particles are easily pulverized, resulting in poor cycling performance of Sn. The authors uniformly deposited Sn nanoparticles on the Ni coating and then wrapped a thin carbon layer outside to obtain multilayer core-shell nanorods composed of TMV-Ni-Sn-C. Meanwhile, they vertically arranged nanorods in an orderly fashion on a stainless steel substrate, and the gap between the nanorods will effectively relieve the strain caused by volume expansion. Compared with the ordinary 2D Sn film, this nanorod provides great electrochemical properties as an anode for SIBs. As shown in Figure 9D, the ordinary 2D Sn thin film rapidly decays to zero after ten cycles, while the core-shell Sn nanorods have a stable capacity of 400 mAh g^{-1} after 150 cycles. Additionally, they also explored the influence of carbon coating on Sn nanorods. The experimental results showed that the capacity of Sn

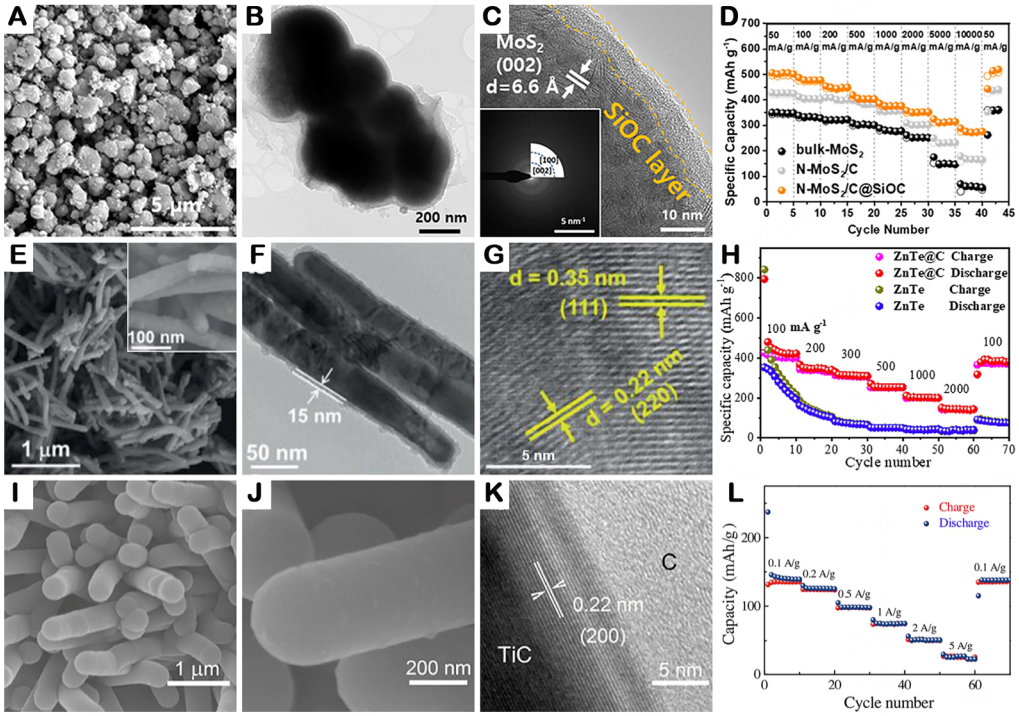

Figure 8. (A) SEM, (B) TEM, and (C) HR-TEM images and (D) rate performance of core-shell MoS_2/SiOC[83]. (E) SEM, (F) TEM, and (G) HR-TEM images and (H) rate performance of core-shell ZnTe@N doped carbon nanowire(ZnTe@C)[84]. (I) SEM, (J) TEM, and (K) HR-TEM images and (L) rate performance of core-shell TiC/C[85].

nanorods without carbon coating decreases to about 100 mAh g^{-1} after 50 cycles because the carbon coating can efficiently inhibit the reunion of Sn. Li *et al.* designed a 3D core-shell structure BTO@SnO_2@P-C composite composed of a barium titanate core, tin dioxide shell, and phosphorus-doped carbon shell [Figure 9E-G][87]. SnO_2 is an alloy-based anode with a very serious volume expansion (420%), which also brings poor cycling performance and rate performance. The coating of the carbon layer and the support of the $BaTiO_3$ (BTO) core significantly alleviate the volume expansion of SnO_2. In addition, under the *in-situ* polarization of the external electric field and the compressive stress of the SnO_2 shell, BTO generates a unique built-in electric field (BIEF) and greatly increases the diffusion rate of sodium ions. Therefore, the core-shell structure BTO@SnO_2@P-C material exhibits excellent cycling performance and fast charging ability as an anode material for SIBs. At 100 A g^{-1}, it exhibits more than twice the reversible capacity (618.8 mAh g^{-1}) compared to SnO_2@P-C (289.1 mAh g^{-1}) [Figure 9H and I]. At the same time, BTO@SnO_2@P-C provides an ultra-long cycle life of more than 10,000 cycles (10 A g^{-1}) and fast kinetics (up to 99% rechargeable in 1 min). Yang *et al.* reported a multi-core-shell structured Bi@N-doped carbon nanospheres for sodium and potassium-ion batteries [Figure 9J-L][88]. When Bi is used as an anode material, the particles will be crushed due to the huge volume expansion, which will lead to the thickening of the SEI film. Constructing a reasonable 3D architecture is one of the effective means to improve the performance of Bi electrodes. The Bi@N-C nanospheres are composed of N-doped carbon shells (~30 nm) and multiple Bi cores with different sizes. The carbon shell effectively reduces the volume expansion of Bi and the formation of SEI films on Bi nanospheres. In SIBs, Bi@N-C exhibits excellent rate performance and cycling performance. At 10 A g^{-1}, Bi@N-C can maintain a reversible capacity of more than 200 mAh g^{-1} and last for more than 2,000 cycles [Figure 9M]. When the current density is increased to 100 A g^{-1}, Bi@N-C still provides a reversible capacity of more than 170 mAh g^{-1} (6.4 s charge/discharge). These excellent properties also benefit from the extremely short diffusion distance brought by Bi nanoparticles (multi and small). At the same time, the N-doped carbon shell enhances the conductivity and Na/K transport activity.

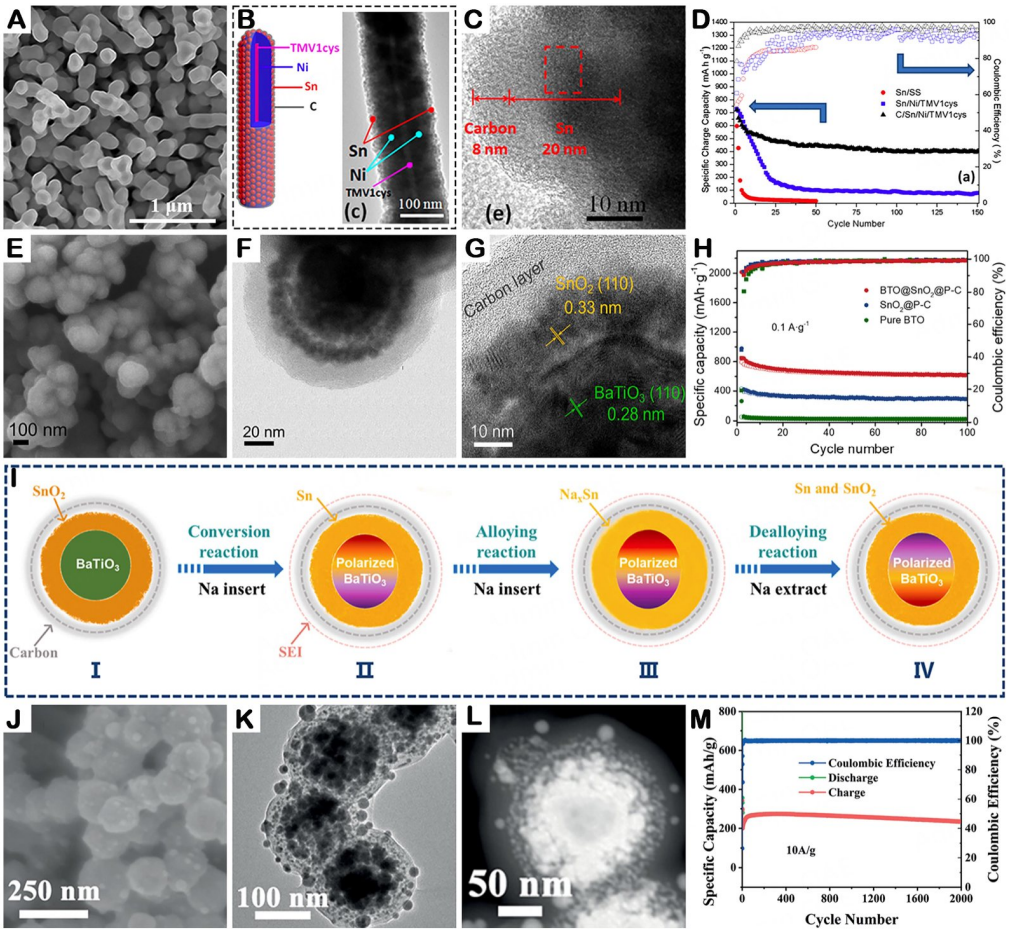

Figure 9. (A) SEM, (B) TEM, and (C) HR-TEM images and (D) cycling performance of multi-shell Sn nanorods (TMV-Ni-Sn- C)[86]. (E) SEM, (F) TEM, (G) HR-TEM images and (H) cycling performance of multi-shell BTO@SnO2@P-C, (I) schematic illustration of the sodiation mechanism of BTO@SnO2@P- C[87]. (J) SEM and (K and L) TEM images and (M) cycling performance of multi-core-shell Bi@N-doped carbon nanospheres[88].

Hierarchical core-shell structure

As mentioned earlier, hierarchical structures refer to a complex 3D arrangement, usually constructed from low-dimensional simple structures. For core-shell structures, the grading usually appears as the shell consists of low-dimensional or more complex nanostructures. Because the core and shell are tightly bonded in the core-shell structure, the shell structure is usually easier to control. For example, the uniform growth of a 3D architecture material on the surface of the substrate material is a common strategy for constructing a hierarchical core-shell structure. In recent years, MOF materials have become an expected precursor for SIB electrode materials due to their excellent modification ability, regular polyhedron morphology, and simple synthesis methods. Generally, MOF can be synthesized in a simple solution and uniformly wrapped on the surface of the matrix material. Not only that, MOF can maintain its original skeleton and morphology and even selectively leave elements during subsequent processing. Therefore, MOF plays an important role in the strategy of designing complex core-shell structures.

Huang *et al.* designed a hierarchical core-shell Bi_2S_3@Co_9S_8 composite for SIB anodes. Bi_2S_3 has a high theoretical specific capacity but poor cycling performance[89]. However, the commonly used carbon coating method has little improvement in the capacity decay of Bi_2S_3. Therefore, the authors used Co-based MOF

(ZIF-67) to coat BiOBr spheres and obtained Bi_2S_3@Co_9S_8 composites after vulcanization and sintering. As shown in Figure 10A-E, the hierarchical core-shell structured material with Bi_2S_3 spheres as the core and multi-cavity Co_9S_8 as the shell was successfully prepared and exhibited good cycling and rate performance (595 mAh g^{-1} at 0.5 A g^{-1} after 800 cycles). Due to the regular morphology and stable skeleton structure of MOF, ZIF-67 uniformly covered the surface of BiOBr spheres and formed a unique 3D architecture after sintering. Thanks to this hierarchical core-shell structure, Bi_2S_3@Co_9S_8 composites have good buffering capacity for volume changes. In addition, the multi-cavity structure of Co_9S_8 provides a larger specific surface area and a shorter ion diffusion path. Xie *et al.* reported a hierarchical core-shell structure of carbon and $MoSe_2$ composites[90]. Unlike the usual carbon coating, their strategy to realize the core-shell structure is to allow the lamellar $MoSe_2$ to grow in situ on the carbon skeleton, which is obtained by sintering the MOF. ZIF-8 with a larger size (~800 nm) was prepared in this paper and maintained a regular polyhedron morphology after sintering. Subsequently, $MoSe_2$ is uniformly grown on the carbon polyhedron by a hydrothermal method and exhibits a hierarchical structure [Figure 10F]. The lamellar structure of $MoSe_2$ effectively alleviates the volume expansion during sodium storage and provides more active sites. In addition, the carbon skeleton obtained by sintering the MOF brings good electrical conductivity and porosity and prevents the aggregation and dissolution of selenides. Therefore, compared with pure $MoSe_2$, the hierarchical core-shell structured $MoSe_2$/C anode material exhibits excellent rate performance and cycle stability in SIBs (436 mAh g^{-1} after 500 cycles) [Figure 10G]. This new carbon composite strategy based on MOF opens the way for SIB conversion anode materials. Hierarchical core-shell structures also have great potential in sodium-ion hybrid capacitors (SIHCs). SIHCs are a special energy storage system that combines the high energy density of batteries and the high power density of supercapacitors. However, it also faces problems such as dynamic imbalance, difficulty in matching positive and negative poles, and poor rate performance. In order to construct flexible electrode materials with stable structures and excellent electrochemical performance, Wang *et al.* prepared core-shell MoS_2/porous carbon nanofiber (PCNF) materials [Figure 10H-K][91]. In this structure, the porous carbon nanotube core can provide a certain flexibility and resist the mechanical stress during charge and discharge, while the MoS_2 shell assembled by 2D nanosheets exhibits good sodium storage performance (~400 mAh g^{-1} after 5,000 cycles in 2 A g^{-1}).

Yolk-shell structure

The yolk-shell structure has the following advantages: (i) Core-shell separation: the cavity has a good buffering effect on the volume expansion of the core during the electrochemical process; (ii) thin shell and small core: shorten the ion diffusion distance, increase the specific surface area, which is conducive to rapid sodiation/desodiation; and (iii) Confinement effect: The shell has a limiting effect on the active area of the nucleus, effectively preventing the pulverization and agglomeration of the nucleus and enhancing the cycle stability.

Single yolk/shell structure

The simplest yolk-shell structure consists of a shell and a core, similar to an egg. The cavity between the shell and the core resembles the protein between the eggshell and the yolk, so it is called the yolk-shell structure. Compared with core-shell structures, the construction strategy of yolk-shell structures is more complex, which usually includes coating, etching, and sintering.

Wang *et al.* reported a yolk-shell FeS@C anode material for high-performance SIBs[92]. FeS is a common LIB and SIB anode material due to its high theoretical capacity, low cost, and controllable microstructure. However, the conductivity of FeS and the volume expansion during sodium storage prevent its further application. Wang and others have chosen classic carbon-coating methods to solve these problems, but their strategy is different from others. As shown in Figure 11A-C, they obtained yolk-shell structured Fe_3O_4@C by etching the SiO_2 template and maintained the morphology during subsequent vulcanization and high

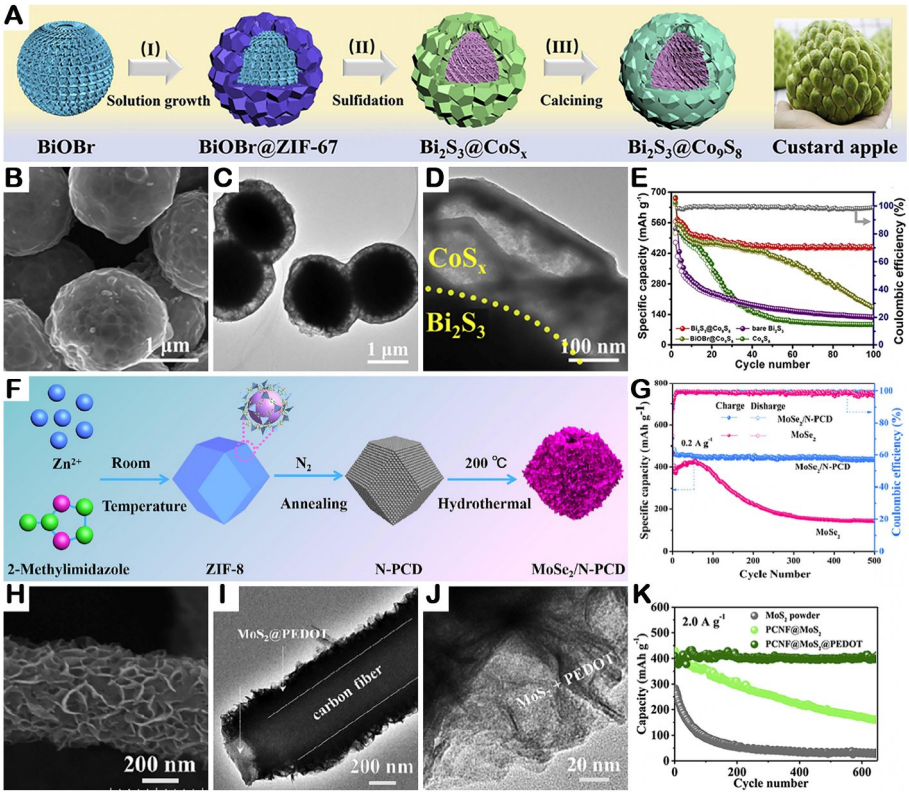

Figure 10. (A) Schematic of the synthesis, (B) SEM, (C) TEM, and (D) HR-TEM images, and (E) cycling performance of hierarchical core-shell Bi_2S_3@Co_9S_8 [89]. (F) Schematic of the synthesis and (G) cycling performance of hierarchical core-shell $MoSe_2$/N-PCD [90]. (H) SEM, (I) TEM, and (J) HR-TEM images and (K) cycling performance of hierarchical core-shell MoS_2/PCNF [91].

temperature sintering. It is worth mentioning that the yolk-shell FeS@C exhibits superior rate performance and cycle life than both pure FeS and core-shell FeS/C (488 mAh g^{-1} after 300 cycles) [Figure 11D]. In fact, the performance advantage of the yolk-shell FeS@C is due to its unique cavity that can accommodate a volume-expanding FeS sphere. Their work demonstrated that the yolk-shell structure has a unique advantage over the core-shell structure and also provides a new strategy for constructing 3D architectures for conversion and alloy-based anode materials. Sun *et al.* prepared a yolk-shell SnS_2@C anode material for SIBs and PIBs using a green and simple method[93]. In this paper, the sodium storage mechanism of SnS_2 is studied by in situ Raman technique. The results successfully confirmed that the two steps of conversion reactions and alloying reactions exist simultaneously. Therefore, SnS_2 exhibits considerable theoretical specific capacity, but its unique sodium storage process also brings huge volume expansion. The yolk-shell SnS_2@C was prepared by three steps: polydopamine (PDA) coating and high temperature carbonization and vulcanization, and the SnS_2 spheres were perfectly confined in the carbon box [Figure 11E and F]. Compared to SnS_2/C, yolk-shell SnS_2@C exhibits better rate performance (362 mAh g^{-1} at 5 A g^{-1}) and cycle stability (~300 mAh g^{-1} after 500 cycles at 2 A g^{-1}) [Figure11I]. These results indicate that yolk-shell structures are one of the best strategies for solving volume expansion and polysulfide dissolution. Doping shell is a realizable and efficient modification method to improve sodium storage performance. Xiao *et al.* prepared a yolk-shell $SnSe_2$@C anode material with Se doping in the shell for SIBs[94]. Firstly, the yolk-shell SnO_2@C was obtained by the classical SiO_2 template method, and then the doping of Se in the carbon shell was realized by high temperature selenization [Figure 11G and H]. Density functional theory (DFT) proves that the incorporation of Se forms a Se-C bond in the carbon shell, which successfully improves the binding ability between the $SnSe_2$ core and the carbon shell and improves the conductivity of the carbon shell.

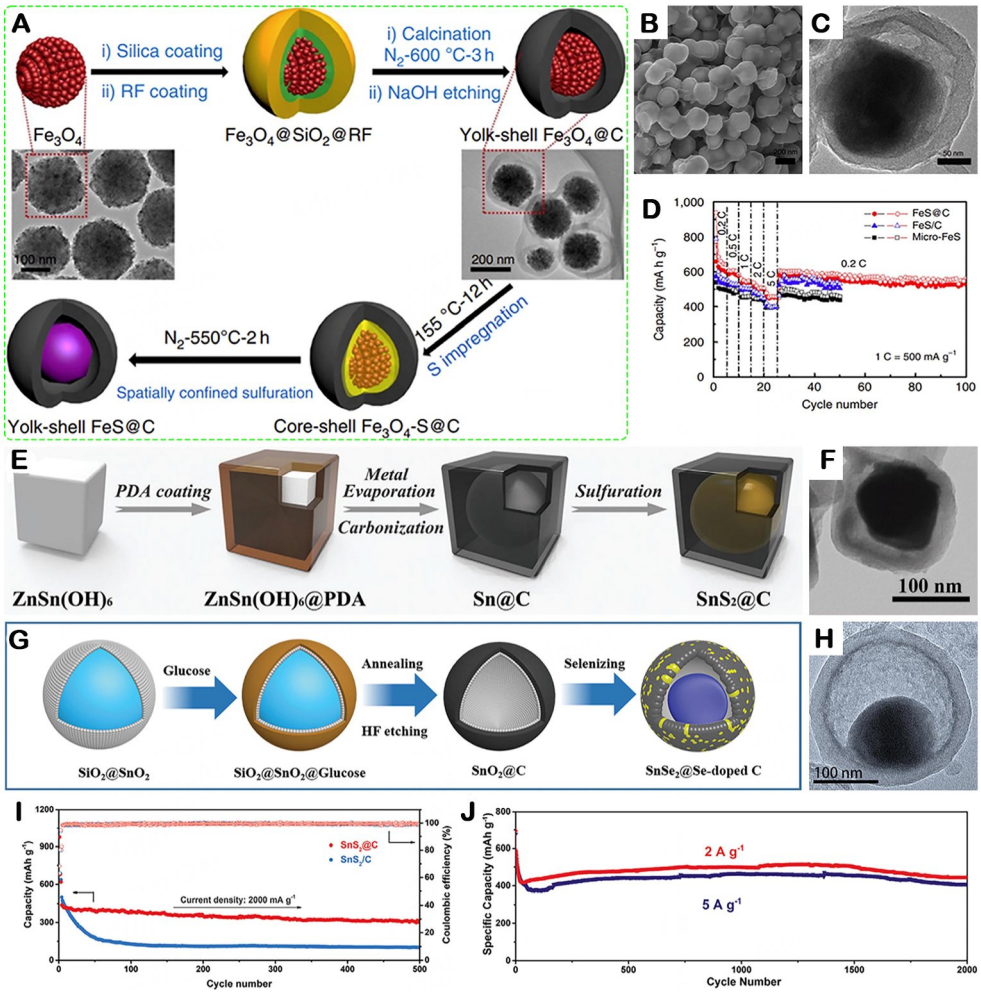

Figure 11. (A) Schematic of the synthesis, (B) SEM and (C) TEM images, and (D) rate performance of yolk-shell FeS@C[92]. (E) Schematic of the synthesis, (F) TEM images, and (I) cycling performance of yolk-shell SnS_2@C[93]. (G) Schematic of the synthesis, (H) TEM images, and (J) cycling performance of yolk-shell $SnSe_2$@C[94].

Therefore, the prepared yolk-shell $SnSe_2$@Se-C material exhibits superior cycle stability and sodium storage kinetics. The ratio of Se doping is directly related to the reaction time. $SnSe_2$@Se-C, with the optimal doping ratio, exhibits a specific capacity of about 400 mAh g^{-1} at 5 A g^{-1} after 2,000 cycles [Figure 11J]. This work provides useful strategies and unique insights for doping modification of single yolk-shell structures.

Multi yolk/shell structure

Multiple yolk/shell structures have multiple yolks or multi-shell structures, which can bring different performances. Li *et al.* reported a yolk-shell V_2O_3/C composite with multiple shells for LIBs and SIBs[95]. Transition metal oxide (TMO) anodes usually improve their poor conductivity and reaction kinetics by optimizing electrode structures, coupling with other conductive materials or other methods. Based on that, the authors designed a simple solvothermal route to prepare multilayer yolk-shell V_2O_3/C, and the number of shells can be controlled by reaction time [Figure 12A]. The prepared V_2O_3/C composite consists of several V_2O_3 shells and a V_2O_3 core, and the V_2O_3 shell is uniformly covered with a 2 nm thick carbon coating [Figure 12B and C]. In this unique multilayer yolk-shell structure, a thin and porous V_2O_3 layer allows sodium ions to pass quickly, a carbon coating enhances the conductivity of the overall skeleton, and a stable yolk-shell structure effectively relieves volume expansion. As an anode material for SIBs, such a

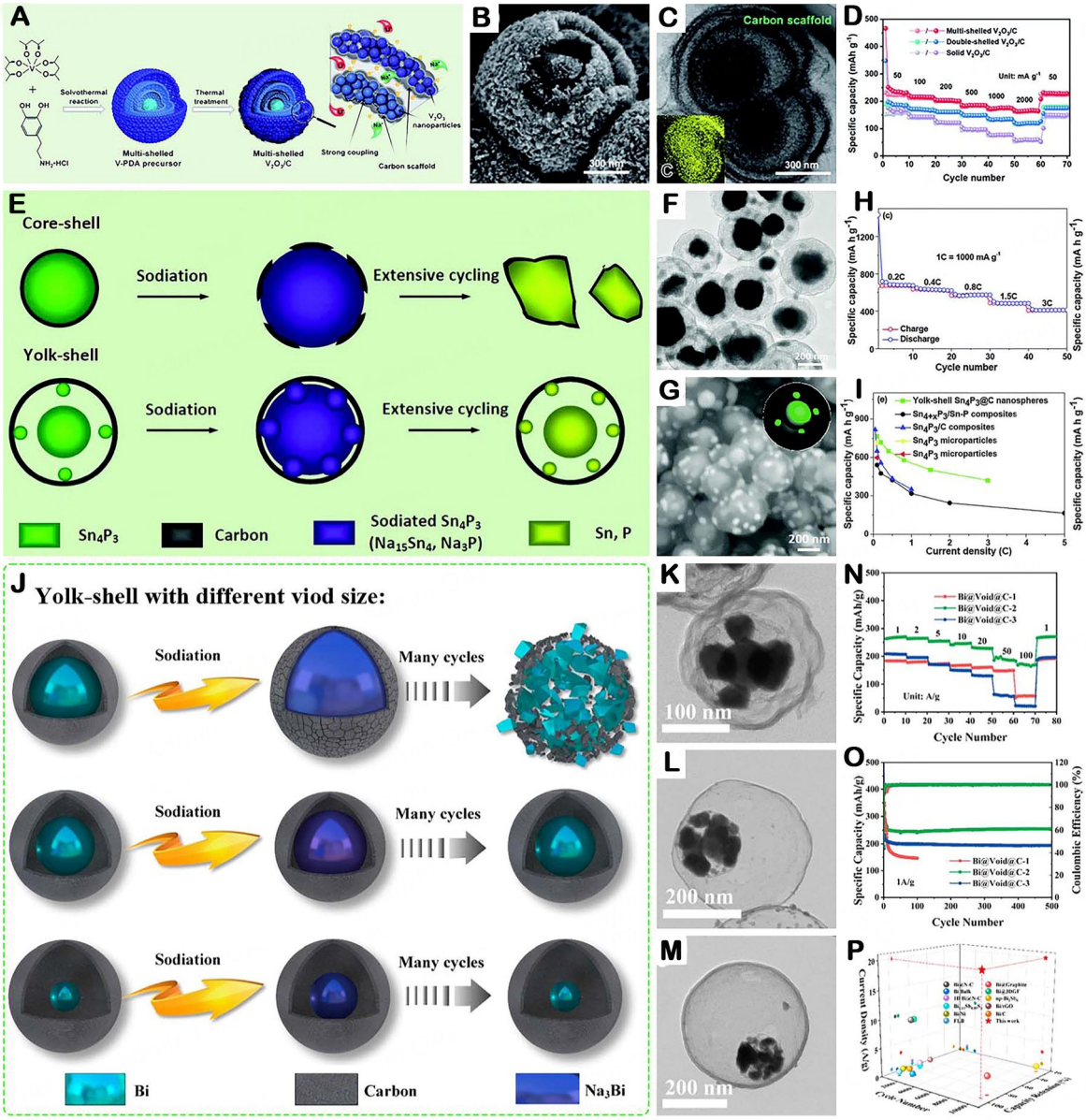

Figure 12. (A) Schematic of the synthesis, (B) SEM and (C) TEM images, and (D) rate performance of yolk-multi-shell V_2O_3/C[95]. (E) Schematic illustration of the sodiation process in core-shell Sn_4P_3@C and multiyolk-shell Sn_4P_3@C. (F) TEM and (G) SEM images (H) cycling performance and (I) rate performance of multiyolk-shell Sn_4P_3@C[96]. (J) Schematic illustration, (K-M) TEM images, and (N-P) electrochemical performance of Bi@Void@C with different void sizes[98].

delicate structure brings a reversible capacity of 173 mA h g^{-1} at 1 A g^{-1} after 2,000 cycles and enhanced rate performance [Figure 12D]. The success of V_2O_3/C composites provides a strategy for the preparation of multilayer yolk-shell structured anode materials and reveals the great potential of multilayer structures in improving reaction kinetics.

Liu *et al.* reported a multiyolk-shell Sn_4P_3@C nanosphere for SIBs [Figure 12E-G][96]. As an intermetallic compound anode material, Sn_4P_3 has higher theoretical volume capacity and conductivity than Sn and P. However, Sn_4P_3 suffers from the same volume expansion problem. The ingenious design of the yolk-shell structured Sn_4P_3@C alleviates the volume expansion to some extent. In the typical synthesis process,

SnO_2@C with double-shell hollow structures was first prepared and transformed into Sn_4P_3@C with multi-yolk structure after hydrogen reduction and phosphating. In the tests of rate performance (0.2~3 A g^{-1}), Sn_4P_3@C delivers a reversible capacity of 505 mAh g^{-1} at 1.5 A g^{-1}. At the same time, Sn_4P_3@C exhibits good cycling performance (360 mAh g^{-1} after 400 cycles), demonstrating the excellent resistance of the yolk-shell structure to volume expansion [Figure 12H and I]. Prior to this, Qian *et al.* reported a core-shell structured Sn_4P_3/C nanocomposite[97]. At 1 A g^{-1}, the reversible capacity is only 349 mA g h^{-1}. The results showed that the yolk-shell structure has better performance than the core-shell structure because the yolk-shell structure provides a cavity to alleviate volume expansion and the multi-yolk structure provides more sodium storage sites.

For the yolk-shell structure, the size of the cavity has an important influence on the electrochemical performance of the material because the cavity determines its ability to alleviate the volume expansion. Yang *et al.* proved this view by adjusting the cavity volume between the Bi yolk and the C shell in the yolk-shell Bi@C structure[98]. By adjusting the amount of tetraethoxysilane (TEOS) and phenolic resin (RF), three yolk-shell Bi@C with cavity volume ratios of 1, 10, and 20 were prepared [Figure 12J]. The results showed that the Bi@C-2 anode material [Figure 12K] with medium cavity volume exhibits the best sodium storage performance (198 mAh g^{-1} after 10,000 cycles at 20 A g^{-1}). Bi@C-1 with a smaller cavity volume [Figure 12L] exhibits a faster capacity decay in cycling tests (146 mAh g^{-1} after 100 cycles at 1 A g^{-1}) due to the continuous expansion of the volume of Bi during sodiation, which breaks the carbon shell and eventually collapses the structure. On the other hand, Bi@C-3, with a larger cavity volume [Figure 12M], shows good cycling performance, which is similar to Bi@C-1. However, the rate performance of Bi@C-3 is much worse than that of Bi@C-1 because the cavity volume is too large and the sodium ion diffusion distance is greatly increased [Figure 12N-P]. The results prove the necessity of regulating the cavity volume of yolk-shell structures and provide a valuable scheme for its optimized design strategy.

Hierarchical yolk/shell structure

The graded yolk-shell structure is usually composed of a graded shell or a graded core. Unlike the core-shell structure, the shell and core of the yolk-shell structure are separate, so the two can form a hierarchical structure.

Chen *et al.* reported a yolk-shell Fe_7Se_8@C@$MoSe_2$ with hierarchical shell structures for SIBs[99]. The problems of large volume expansion and low conductivity of iron selenide anode materials are usually solved by carbon coating, but more progress is still needed. The authors proposed a strategy to further release the volume expansion stress by *in-situ* growth of lamellar $MoSe_2$ on the basis of iron selenide/carbon composites. In a typical synthetic route [Figure 13A], yolk-shell structured Fe_3O_4@C was first prepared, and then, MoS_2 nanosheets were uniformly grown on its surface by a solvothermal method and finally transformed into Fe_7Se_8@C@$MoSe_2$ composites by high temperature selenization. As shown in Figure 13B and C, Fe_7Se_8@C@$MoSe_2$ is composed of Fe_7Se_8 yolk, carbon shell, and 2D $MoSe_2$ decoration from inside to outside. The finite element (FE) simulation revealed a rule suitable for the hierarchical yolk-shell structure; that is, the construction of 2D nanosheet arrays on the surface of the yolk-shell structure can further inhibit the sodium-induced fracture in the shell. Fe_7Se_8@C@$MoSe_2$ shows enhanced electrochemical performance (345 mAh g^{-1} at 1.0 A g^{-1} after 600 cycles) due to the pressure release effect of lamellar $MoSe_2$ and the heterogeneous interface of C@$MoSe_2$ [Figure 13D]. The results provide strong theoretical support for the construction strategy of hierarchical yolk-shell structures and prove their great potential in battery materials.

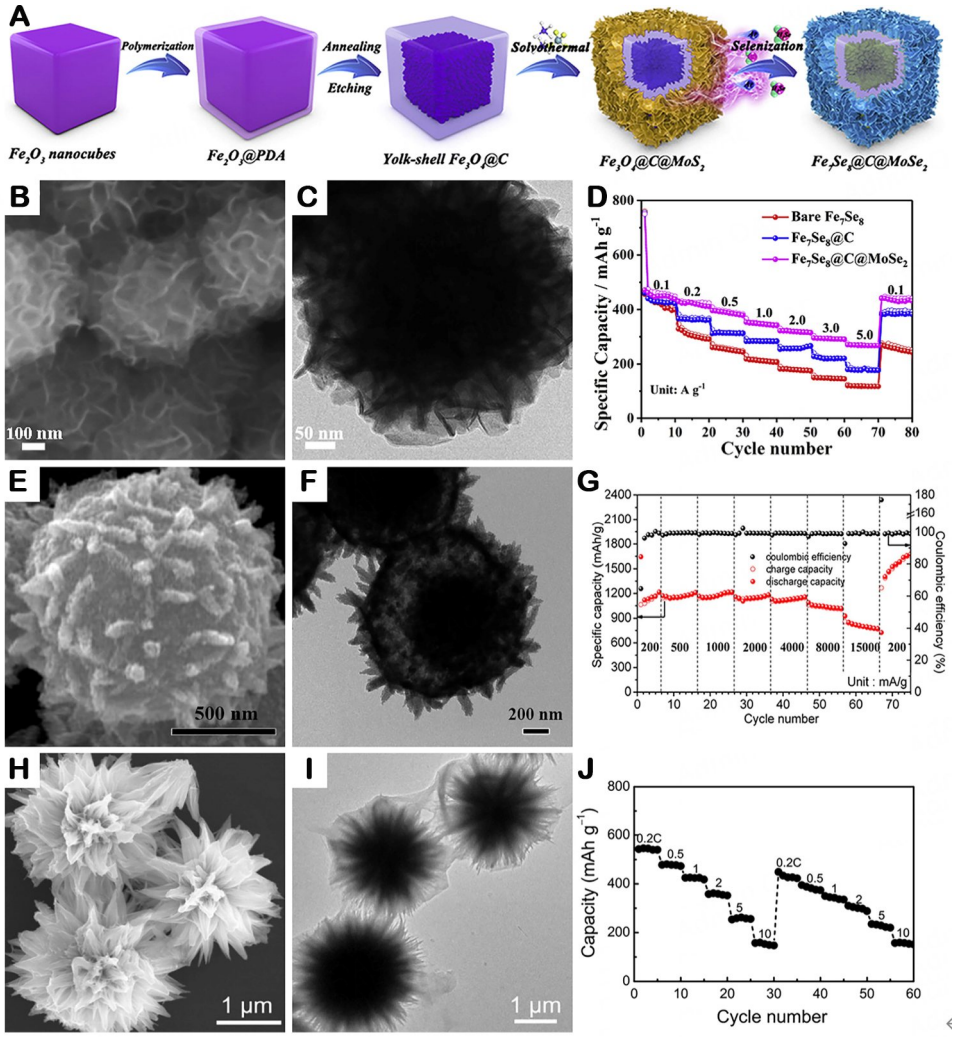

Figure 13. (A) Schematic of the synthesis, (B) SEM and (C) TEM images, and (D) rate performance of hierarchical yolk-shell Fe_7Se_8@C@$MoSe_2$[99]. (E) SEM and (F) TEM images and (G) rate performance of hierarchical yolk-shell NiO/Ni/graphene[100]. (H) SEM and (I) TEM images and (J) rate performance of hierarchical yolk-shell Bi_2S_3-PPy[101].

In addition to 2D nanosheets, other types of complex structures can also be used to modify the surface of yolk-shell structures. For example, Zou *et al.* reported a hierarchical yolk-shell NiO/Ni/graphene composite[100]. Firstly, Ni-MOF with hierarchical yolk-shell structures was successfully prepared by adjusting the amount of polyvinyl pyrrolidone (PVP). Subsequently, the initial morphology was maintained during two annealings and core-shell NiO/Ni/graphene nanocrystals were formed on the shell surface [Figure 13E and F]. In fact, the formation of yolk-shell Ni-MOF is a typical Ostwald ripening process. It is called a hierarchical structure because the surface of the yolk shell is uniformly distributed with nanocrystals that are smaller than 5 nm. These nanocrystals are composed of ultrathin graphene shells and Ni/NiO cores. Graphene-coated nanocrystals enhance the conductivity of NiO and accelerate the transport rate of Na^+, and the well-graded yolk-shell structure resists volume expansion during cycling. The results of electrochemical tests showed that the hierarchical yolk-shell NiO/Ni/graphene composite provides excellent rate performance (207 mAh g^{-1} at 2 A g^{-1}) [Figure 13G]. The MOF-based strategy for constructing hierarchical yolk-shell structures provides innovative suggestions for transition metal nanoparticles.

In the graded yolk-shell structure, the graded core structure also occupies a place. Liang *et al.* reported a bio-inspired hierarchical yolk-shell Bi_2S_3-PPy composite for LIBs and SIBs[101]. As an anode for conversion reactions, Bi_2S_3 cannot exhibit high reversible capacity due to its huge volume expansion. Carbon coating is a common solution, but it usually requires a high temperature pyrolysis process, which sometimes leads to the collapse of the designed structure or the reduction of the active material. Therefore, the authors proposed a strategy for PPy coating of hierarchical Bi_2S_3 materials without high temperature heat treatment. The hierarchical Bi_2S_3 was obtained by a simple solvothermal method, and then, PPy films were formed outside the Bi_2S_3 core by vapor phase polymerization. As shown in Figure 13H and I), the Bi_2S_3 core is assembled by ultrathin nanowires with a diameter of 5-10 nm, and the PPy film is uniformly covered on its surface. In the electrochemical performance test, Bi_2S_3-PPy exhibits better cycling performance (about 400 mAh g^{-1} after 100 cycles) and rate performance (335 mAh g^{-1} at 3.125 A g^{-1}) [Figure 13J], while bare Bi_2S_3 only provides a reversible capacity of about 100 mAh g^{-1} after 100 cycles. The results showed that this hierarchical core structure does not produce excessive SEI films and polysulfide dissolution due to the coating of PPy films while providing a large specific surface area and fast ion transport rate. In addition, the soft PPy film plays a role in improving conductivity and buffering volume expansion.

The terms "hollow", "core-shell", and "yolk-shell" are frequently interchanged and misused in many research papers. In this review, we attempt to provide clear definitions of these three structures. It is necessary to distinguish them because they exhibit different properties. Only by deeply understanding the differences between these three materials can we better design and utilize them. Compared with core-shell structures, hollow structures and yolk-shell structures both have unique advantages in alleviating volumetric expansion, but their energy density is generally lower than core-shell structures, which limits their commercial application. Although the theoretical energy density of the core-shell structure is high, the utilization rate of the core is not satisfactory due to slow kinetics. The yolk-shell structure has comprehensive advantages, but the construction method of yolk-shell structures is usually tedious. In the future, finding simple methods for constructing 3D architectures may become a research focus.

Porous structure

Porous structures are quite common 3D architectures and often coexist with other types of 3D architectures in a material. For example, hollow porous carbon nanospheres and core-shell structures with porous shells are common. However, when the materials exhibit other more concrete 3D structure types, they are usually not classified as porous structures. In this chapter, we will briefly introduce some anode materials dominated by porous structures. Porous materials can be divided into three categories by pore size: microporous materials, mesoporous materials, and macroporous materials.

Porous materials with an average pore size of less than 2 nm are called microporous materials. Microporous materials have received extensive attention in the field of EES due to their abundant and ultra-small pores, the most typical of which is microporous carbon materials. However, porous carbon materials usually face the problem of low ICE due to the uncontrollable formation of SEI films. In order to improve the ICE and sodium storage capacity of porous carbon materials in SIBs, Feng *et al.* proposed a strategy of sulfur coating and N, S co-doping[102]. In a typical synthetic route, N-doped porous carbon (NPC) precursors are synthesized by MOF-based methods. Subsequently, the precursor was calcined with sulfur to achieve sulfur filling in the micropores and boundary S doping [Figure 14A-C]. Compared with NPC, the ICE of N, S co-doped porous carbon (NSPC) increased from 52.9% to 72.3% because the sulfur-filling strategy greatly reduced the specific surface area of micropores. In addition, the addition of S also provides sodium storage capacity and increases the electron/ion exchange rate, so NSPC exhibits enhanced cycling performance (98% capacity retention at 10 A g^{-1} after 700 cycles) and rate performance (233.3 mAh g^{-1} reversible capacity at 10 A g^{-1}) [Figure 14D]. This doping strategy provides a feasible idea for the ICE problem of microporous carbon materials.

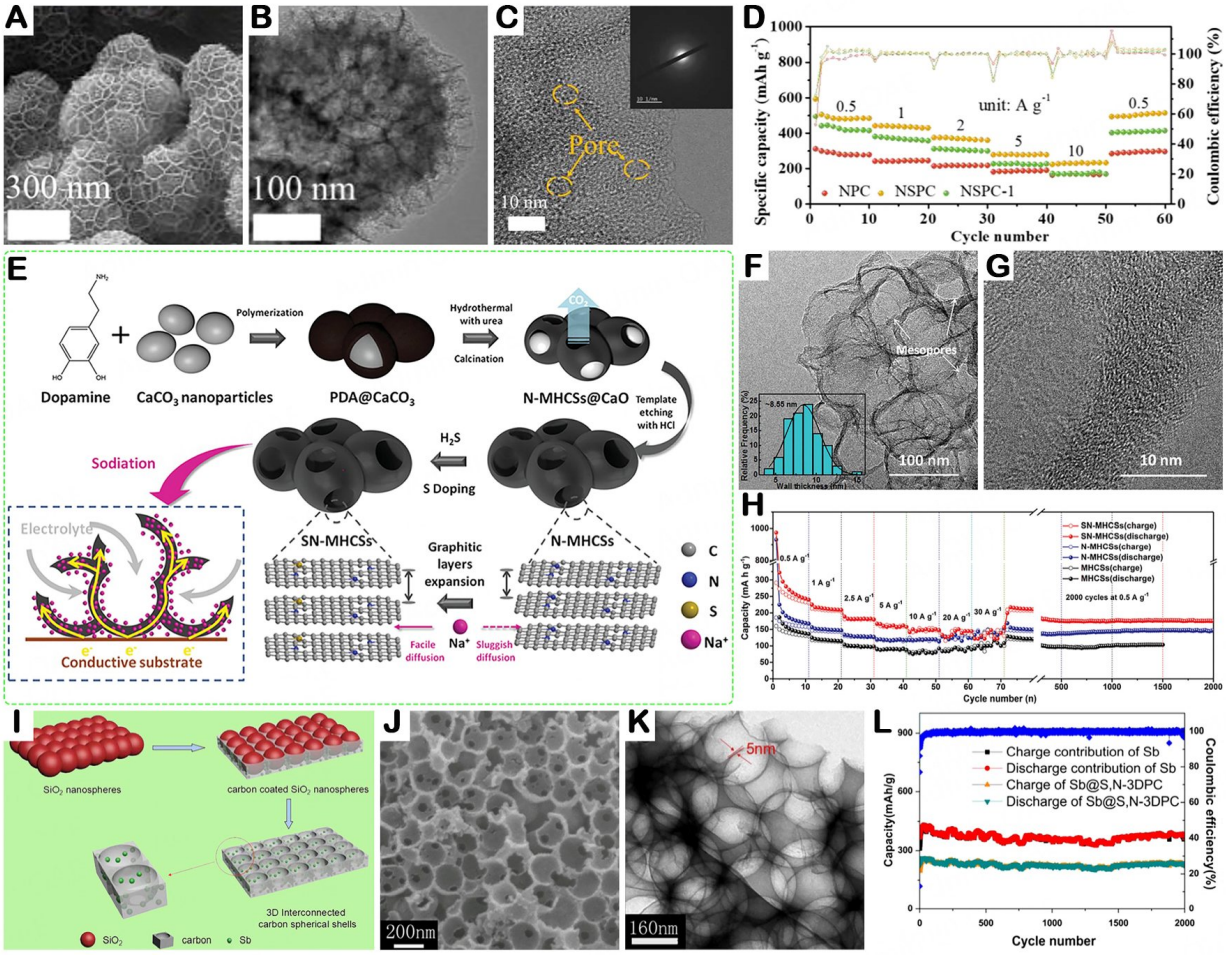

Figure 14. (A) SEM, (B) TEM, and (C) HR-TEM images and (D) rate performance of N, S co-doped microporous carbon (NSPC)[102]. (E) Schematic of the synthesis, (F) TEM and (G) HR-TEM images, and (H) electrochemical performance of S and N co-doped mesoporous carbon spheres (SNMHCSs)[103]. (I) Schematic of the synthesis, (J) SEM and (K) TEM images, and (L) cycling performance of N and S co-doped 3D macroporous carbon (Sb@S, N-3DPC)[104].

The pore size of mesoporous materials is usually between 2 nm and 50 nm. In the case of the same pore volume, the specific surface area of the material will decrease with the increase of pore sizes, which will bring some different characteristics. Ni *et al.* reported a S and N co-doped mesoporous carbon sphere for high-performance SIB anode materials[103]. Mesoporous carbon spheres are synthesized using PDA as carbon sources, calcium carbonate as a template, and pore-forming agents. Calcium carbonate decomposes at high temperatures to form carbon dioxide, and then carbon dioxide will break through the carbon wall to form mesopores [Figure 14E-G]. The mesoporous structure can provide a large specific surface area, allowing rapid exchange of Na^+ and reducing the volume expansion stress to some extent. In addition, N and S are doped at the same time as high temperature sintering. The results showed that the doping of N and S brings larger interlayer spacing and more functional groups and lattice defects to the mesoporous carbon anode while maintaining the initial mesoporous carbon morphology. Taken together, the S and N co-doped mesoporous carbon anode exhibits excellent cycling and rate performance, providing a specific capacity of 180 mAh g^{-1} even after 7,000 cycles at 20 A g^{-1} [Figure 14H]. This strategy of constructing mesoporous structures is unique and has guiding significance for the modification of 3D carbon materials.

Macroporous structures have large pore sizes (> 50 nm), which are common on larger substrates rather than nanomaterials. For example, Yang *et al.* prepared a macroporous carbon material for SIBs using SiO_2 as a template[104]. As shown in Figure 14I-K, this carbon material is no longer composed of dispersed individual micro/nanoparticles but consists of a carbon matrix and uniform macropores, resembling the structure of a sponge. Under the action of SiO_2 spheres, the macropores appear as quasi-spherical pores (about 200 nm) in the carbon matrix, thus forming a 3D interconnected macroporous carbon skeleton. Then, numerous Sb nanoparticles are encapsulated in the carbon skeleton, which can greatly alleviate the volume expansion of Sb and enhance the conductivity. Finally, N and S co-doped 3D macroporous carbon materials (Sb@S, N-3DPC) embedded with Sb particles were obtained by high temperature calcination. The Sb@S, N-3DPC anode material delivers a reversible capacity of 255 mAh g^{-1} at 2 A g^{-1} after 2,000 cycles [Figure 14L] and retains 160 mAh g^{-1} at a high current density of 5 A g^{-1}. The construction of 3D interconnected macroporous structures provides a new idea for the application of macroporous structures in the field of electrode materials.

The above studies showed that the construction of porous structures is one of the effective ways to improve the anode of carbon-based materials. In general, the porous structure has the following advantages: (i) Large electrode/electrolyte interface: huge specific surface area and high porosity can increase active sites; (ii) Fast ion/electron exchange rate: porous structures accelerate sodium storage reaction kinetics and improve rate performance; and (iii) Excellent structural stability: stable porous structures can effectively buffer the volume expansion. However, the significant disadvantage of porous structures is that it is easy to form excessive SEI films. During the cycles, the pores are in contact with the electrolyte to form an irreversible SEI film, which will cause the pores to clog and affect performance.

Self-assembled nano/micro-structure

In many 3D structure types, hollow structures, core-shell structures, yolk-shell structures, and porous structures are easily identified and classified because of their strong morphological characteristics. However, there are still many reports on the morphology of electrode materials that cannot be strictly classified into one structural type. Those special structures can be called 3D self-assembled nano/microstructures. Three-dimensional self-assembled nano/microstructures possess both the fast ion/electron exchangeability of nanostructures and the strong stability of microstructure and can be divided into two categories according to the way they are assembled: (i) Multiple homogeneous nanostructures self-assemble into microstructures (AA type); and (ii) nanostructures are embedded into another structure to form microstructures (AB type).

AA-type 3D self-assembled nano/micro-structures are very common in SIB anode materials such as flower-like, thread-like, urchin-like, and dandelion-like structures. These structures are usually self-assembled by low-dimensional structures. For example, flower-like structures are self-assembled by 2D nanosheets, and clew-like structures are self-assembled by 1D nanowires. Bai *et al.* reported a self-assembled flower-like $MoTe_2$/C anode material for SIBs[105]. As a Mo-based chalcogenide, $MoTe_2$ usually exhibits the morphology of 2D nanosheets, which is similar to MoS_2 and $MoSe_2$. However, the direct use of lamellar nanomaterials as electrode materials will lead to the accumulation of nanosheets and the collapse of the structure. Self-assembly of nanosheets into flower-like microstructures is an efficient approach to solving the problem. The chelation method was used to prepare flower-like Mo-PDA, and the morphology was maintained during the subsequent oxidation and tellurization processes. As shown in Figure 15A and B, a large number of ultrathin $MoTe_2$/C nanosheets self-assembled into flower-like structures. This structure retains the large specific surface area and fast electron/ion exchange rate of the nanosheets while also improving the stability of the structure. The results showed that the flower-like $MoTe_2$/C exhibits excellent rates and cycling performance (190 mAh g^{-1} at 1 A g^{-1} after 3,000 cycles) [Figure 15C]. In addition, the pH level and telluride temperature have an influence on the electrochemical properties of flower-like $MoTe_2$/C. This work proves

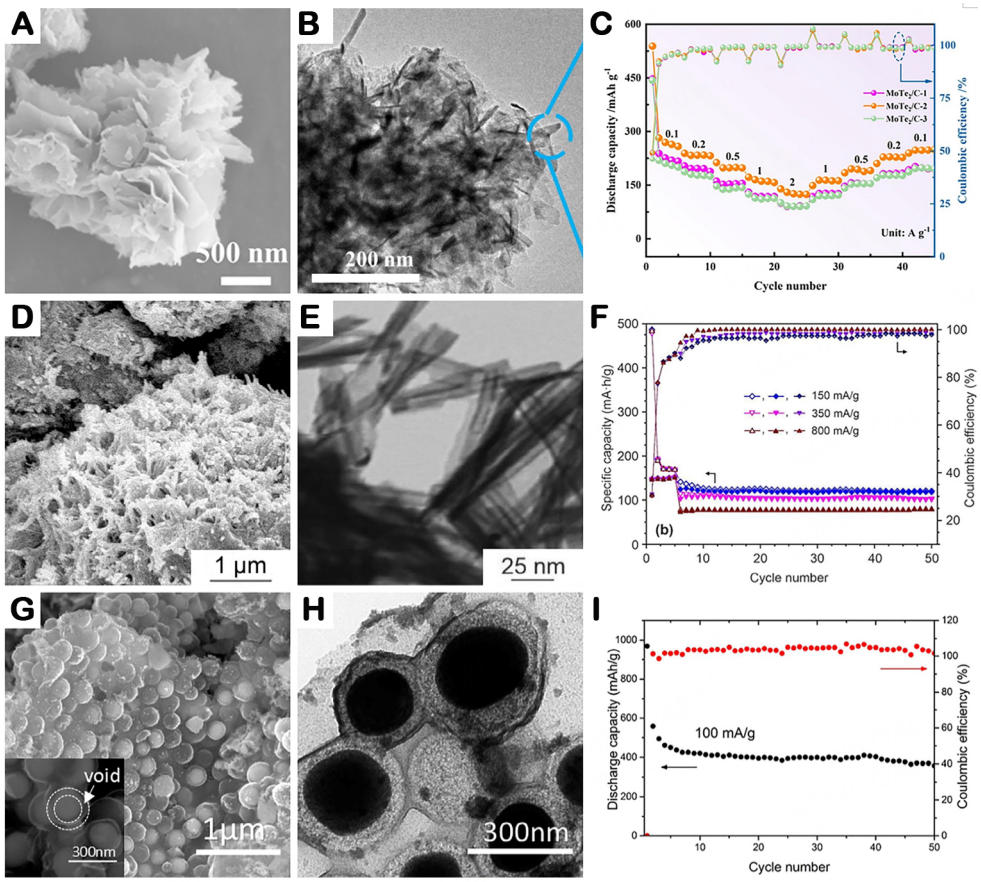

Figure 15. (A) SEM and (B) TEM images and (C) rate performance of self-assembled flower-like $MoTe_2/C$[105]. (D) SEM and (E) TEM images and (F) rate performance of self-assembled monoclinic $Na_2Ti_3O_7$[106]. (G) SEM and (H) TEM images and (I) cycling performance of self-assembled Eggette-like Sn@C[107].

the great effect of self-assembly strategies on improving cycle stability and provides ideas for the modification of self-assembled structures. Opra *et al.* prepared a self-assembled moss-like $Na_2Ti_3O_7$ for SIB anodes by hydrothermal and annealing methods[106]. $Na_2Ti_3O_7$ mossy clusters are composed of numerous small hollow nanotubes with only several nanometers in diameter [Figure 15D and E]. The special structure brings a huge specific surface area and lots of pores, which is conducive to increasing the ion channels and active sites. Additionally, the stability of this self-assembled structure was proved by high temperature experiments (350 °C). The self-assembled moss-like $Na_2Ti_3O_7$ exhibits good cycling and rate performance (95 mAh g^{-1} at 350 mA g^{-1} after 200 cycles) [Figure 15F]. The self-assembly strategy may help $Na_2Ti_3O_7$ show greater potential in the fields of energy, biomedicine, catalysis, and so on. In fact, these examples demonstrate that the self-assembled structure is not a simple mixture of inferiority building blocks but a more stable 3D structure that takes advantage of both nano and micro-structures.

Unlike AA-type structures, AB-type 3D self-assembled nano/microstructures usually contain two or more phases. In addition, the A structure can be not only a single-phase simple structure but also a complex structure such as the core-shell or yolk-shell structure. For example, Li *et al.* embedded yolk-shell Sn@C nanospheres into a carbon matrix to obtain an Eggette-like Sn@C self-assembled anode material for LIB and SIBs[107]. In a typical synthesis process, yolk-shell SnO_2@C nanospheres were first prepared, then SnO_2@C nanospheres and glucose were simultaneously covered on sodium chloride crystals by evaporation, and finally, Sn@C and carbon films were formed by high temperature calcination. The yolk-shell structured

Sn@C has a diameter of about 300 nm; the distance between the Sn core and the carbon shell is about 15 nm, and multiple such yolk-shell structures are embedded on the carbon film, as shown in Figure 15G and H. In this Eggette-like self-assembled structure, the carbon film enhances the stability and conductivity of the overall structure, while the yolk-shell structure alleviates the volume change of Sn. The Eggette-like Sn@C self-assembled anode material provides excellent sodium storage capacity (400 mAh g^{-1} at 0.1 A g^{-1}) [Figure 15I] and cycle stability (200 mAh g^{-1} at 1 A g^{-1} after 1,000 cycles). This report gives an innovative approach to solving the problem of Sn anodes and also provides a strategy for researchers to construct complex self-assembled structures.

All in all, a single structural type or material type faces various problems. The above work showed that 3D self-assembled micro/nanostructures can make up for the defects of a single structure and combine the advantages of multiple materials. Therefore, 3D self-assembled nano/micro-structured anode materials exhibit enhanced capacity and cycling performance. Thus, the construction of 3D self-assembled nano/micro-structures will be one of the future directions of anodes for SIBs.

BRIEF SUMMARIZATION OF METHODS AND PERFORMANCE

In this review, we have mentioned many kinds of anode materials and classified them according to their different structures. As shown in Table 1, varying 3D architectures and materials exhibit distinct performance. In addition, we also pay extra attention to their synthesis methods. Among them, the most commonly used method for constructing 3D structures is the templating method, which includes hard template, soft template, and self-template methods. The hard template method is a simple and stable strategy that can obtain the product with uniform particle size. Meanwhile, the corresponding product structure can be obtained by customizing various template shapes. However, the removal of the hard template requires additional steps, such as acid/alkali etching. These additional steps will lead to higher costs and environmental pollution. The soft template method can remove or transform the template by heating or extraction, while the self-template method does not require additional templates. Under certain conditions, the reactants can be used as their own templates to construct a specific structure. The soft template and self-template methods are more environmentally friendly and cost-effective, but they are usually difficult to accurately control the morphology of products. Besides the template method, hydrothermal, vapor deposition, and calcination methods are also commonly used to construct 3D architectures. It is beneficial to construct complex multi-level structures by using hydrothermal methods, but they are not suitable for large-scale applications. The vapor deposition is commonly used to produce thin-film materials. It is a green method that does not require additional media and high temperature and pressure conditions. Calcination is a kind of high temperature treatment method, such as carbonization and vulcanization. The calcined material often exhibits higher crystallinity, density, and structural stability. Therefore, calcination is always used together with other methods.

CONCLUSION AND OUTLOOK

The composition, structure, and process of materials have a decisive influence on the performance of materials [Figure 16]. In this paper, we summarize the application of 3D architectures in anode materials for SIBs. Many cases have proved that the construction of 3D architectures has a significant impact on improving the sodium storage capacity of anodes. Hollow structures have a large cavity, thin shell, and especially large specific surface area, which improve the rate and cycling performance. Core-shell structures can provide high volumetric energy density and reversible capacity due to the synergistic effect between different materials and abundant heterogeneous interfaces. Yolk-shell structures have a prominent contribution in alleviating volume expansion due to the confinement effect and maintain a good tap density, which can effectively balance the high reversible capacity and long cycle life. Porous structures offer

Table 1. Electrochemical performance and synthesis methods of different 3D architectures

Architectures	Typical samples	Methods	Performance	Ref.
Hollow	Carbon	Hard template	50 mA g^{-1}, 310 mAh g^{-1}	[68]
	Carbon	Self-template	30 mA g^{-1}, 360 mAh g^{-1}	[75]
	MoS_2/SnS	Hard template	10 A g^{-1}, 368 mAh g^{-1}	[79]
Core-shell	MnS/C	Self-template	100 mA g^{-1}, 594 mAh g^{-1}	[82]
	Sn/C	Hard template	50 mA g^{-1}, 400 mAh g^{-1}	[86]
	$MoSe_2$/C	Hydrothermal	200 mA g^{-1}, 464 mAh g^{-1}	[90]
Yolk-shell	SnS_2/C	Soft template	100 mA g^{-1}, 660 mAh g^{-1}	[93]
	V_2O_3/C	Hydrothermal	50 mA g^{-1}, 258 mAh g^{-1}	[95]
	Bi_2S_3/PPy	Vapor deposition	125 mA g^{-1}, 591 mAh g^{-1}	[101]
Porous	Carbon/S	Calcination	500 mA g^{-1}, 592 mAh g^{-1}	[102]
	Carbon	Soft template	20 A g^{-1}, 180 mAh g^{-1}	[103]
	Sb/C	Hard template	100 mA g^{-1}, 482 mAh g^{-1}	[104]
Self-assembled	$MoTe_2$/C	Calcination	250 mA g^{-1}, 580 mAh g^{-1}	[105]
	Sn/C	Self-template	100 mA g^{-1}, 400 mAh g^{-1}	[107]

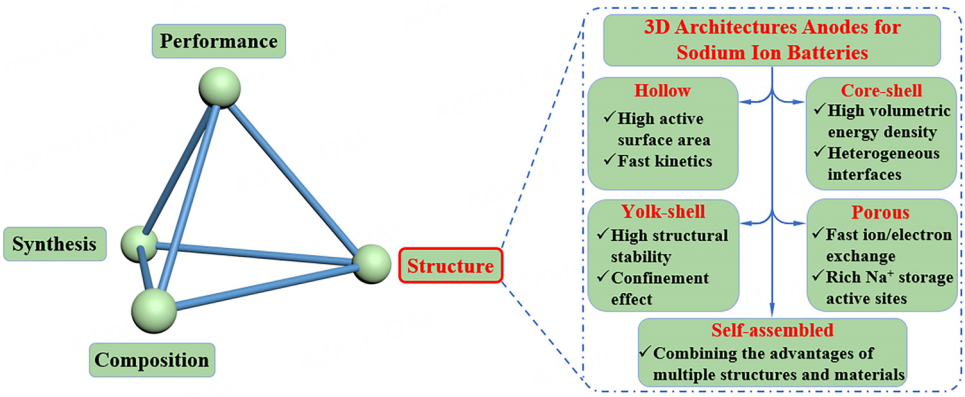

Figure 16. Advantages of different types of three-dimensional architecture anodes for SIBs.

lots of fast sodium ion channels and sodium storage sites, often in conjunction with other structures to improve battery performance. Three-dimensional self-assembled nano/micro-structures can improve the electron/ion exchange capability and structural stability of the anodes by assembling nanostructures into microstructures. While providing unique advantages, each 3D architecture also confronts different problems. For example, hollow structures have a low energy density due to the large cavity, and core-shell structures are not conducive to resisting volume expansion. Yolk-shell structures and porous structures have a large specific surface area, but the larger specific surface area necessitates a greater amount of electrolytes, which will also lead to lower Coulombic efficiency. In addition, a key attribute of high-energy-density batteries is the minimal use of electrolytes. The 3D self-assembly structure faces problems such as cumbersome synthesis routes and uncontrollable assembly processes. Therefore, while benefitting from the performance improvement brought by the 3D architectures, we must also face the various defects they bring. Comprehensively utilizing the advantages of these structures and compensating for their disadvantages will be a research focus in the future. In fact, 3D architectures are constructed to compensate for the defects of simple structures (such as nanospheres, nanowires, and nanosheets) and combine their advantages to enhance material properties. Therefore, the development of SIBs can be effectively promoted by designing 3D architectures of anode materials and utilizing the compatibility of multiple materials or structures.

Compared with the commercial LIBs, the energy density of SIBs is still lower, but their overall cost is higher. Therefore, it is urgent to develop low-cost and high-capacity anodes to improve the competitiveness of SIBs. Although various 3D architecture anode materials have many application examples in the field of SIBs, more efforts are still needed. At present, the primary difficulty is how to optimize the synthesis route. Most of the 3D architectures have complex construction strategies and high energy consumption, which seriously hinders the commercialization of 3D architecture anode materials. At present, most of the construction strategies of 3D architectures are only in the laboratory stage. The development of simple, efficient, and high-yield processes is crucial for the promotion of SIBs. For the commercialized hard carbon anode, poor rate performance and ICE are urgent problems to be solved. Constructing a reasonable 3D architecture may be the future direction of hard carbon anodes. Due to the large specific surface area of the 3D structure anode, irreversible reactions will occur at the interface between the electrode and the electrolyte, resulting in rapid consumption of the electrolyte. In addition, the study of the electrode/electrolyte interface will also be a long-term topic. Another challenge is how to increase the volume energy density. Three-dimensional architectures with a large number of cavities or voids face the problem of low volume energy density exemplified by hollow structures and yolk-shell structures. As one of the potential candidates in the field of energy storage devices and electric vehicles, SIBs must consider the volume energy density of electrode materials more. Therefore, adjusting the ratio of cavity and solid in 3D architecture will be a significant research focus in the coming decades. In addition, due to the ionic radius of sodium, the electrode materials of SIBs have larger volume expansion stress and lower ion transport rates, which means that the electrode materials for SIBs need more effort in structural design. In the future, the development of strategies to construct 3D architectures will be of great significance for the practical application of SIBs.

DECLARATIONS

Authors' contributions

Proposed the topic of this review; reviewed the manuscript: Wu C, Li Y
Wrote the manuscript: Sun YF
Discussed and revised the manuscript: Gong YT, Qiu ZX, Qian J, Wang ZL, Zhang RP, Bai Y

Availability of data and materials

Not applicable.

Financial support and sponsorship

This work was supported by the National Natural Science Foundation of China (Grant Nos. 22279009, 22005033), the National Postdoctoral Program for Innovative Talents (No. BX20180037), and the Beijing Institute of Technology Research Fund Program for Young Scholars (No. XSQD-202108005).

Conflicts of interest

Not applicable.

Ethical approval and consent to participate

Not applicable.

Consent for publication

Not applicable.

REFERENCES

1. Gong Y, Li Y, Li Y, Liu M, Bai Y, Wu C. Metal selenides anode materials for sodium ion batteries: synthesis, modification, and application. *Small* 2023;19:e2206194. DOI
2. Dunn B, Kamath H, Tarascon JM. Electrical energy storage for the grid: a battery of choices. *Science* 2011;334:928-35. DOI PubMed
3. Palacín MR. Recent advances in rechargeable battery materials: a chemist's perspective. *Chem Soc Rev* 2009;38:2565-75. DOI
4. Armand M, Tarascon JM. Building better batteries. *Nature* 2008;451:652-7. DOI PubMed
5. Feng X, Bai Y, Liu M, et al. Untangling the respective effects of heteroatom-doped carbon materials in batteries, supercapacitors and the ORR to design high performance materials. *Energy Environ Sci* 2021;14:2036-89. DOI
6. Yang Z, Zhang J, Kintner-Meyer MC, et al. Electrochemical energy storage for green grid. *Chem Rev* 2011;111:3577-613. DOI
7. Whittingham MS. Lithium batteries and cathode materials. *Chem Rev* 2004;104:4271-301. DOI PubMed
8. Jeong G, Kim YU, Kim H, Kim YJ, Sohn HJ. Prospective materials and applications for Li secondary batteries. *Energy Environ Sci* 2011;4:1986-2002. DOI
9. Wang Z, Yang H, Liu Y, et al. Analysis of the stable interphase responsible for the excellent electrochemical performance of graphite electrodes in sodium-ion batteries. *Small* 2020;16:e2003268. DOI
10. Kim SW, Seo DH, Ma X, Ceder G, Kang K. Electrode materials for rechargeable sodium-ion batteries: potential alternatives to current lithium-ion batteries. *Adv Energy Mater* 2012;2:710-21. DOI
11. Luo W, Shen F, Bommier C, Zhu H, Ji X, Hu L. Na-ion battery anodes: materials and electrochemistry. *ACC Chem Res* 2016;49:231-40. DOI
12. Li Y, Wu F, Li Y, et al. Ether-based electrolytes for sodium ion batteries. *Chem Soc Rev* 2022;51:4484-536. DOI
13. Jin T, Li H, Zhu K, Wang PF, Liu P, Jiao L. Polyanion-type cathode materials for sodium-ion batteries. *Chem Soc Rev* 2020;49:2342-77. DOI
14. Ren H, Li Y, Ni Q, Bai Y, Zhao H, Wu C. Unraveling anionic redox for sodium layered oxide cathodes: breakthroughs and perspectives. *Adv Mater* 2022;34:e2106171. DOI
15. Hwang JY, Myung ST, Sun YK. Sodium-ion batteries: present and future. *Chem Soc Rev* 2017;46:3529-614. DOI PubMed
16. Bruce PG, Scrosati B, Tarascon JM. Nanomaterials for rechargeable lithium batteries. *Angew Chem Int Ed* 2008;47:2930-46. DOI PubMed
17. Fang Y, Luan D, Gao S, Lou XWD. Rational design and engineering of one-dimensional hollow nanostructures for efficient electrochemical energy storage. *Angew Chem Int Ed* 2021;60:20102-18. DOI PubMed
18. Hasa I, Hassoun J, Passerini S. Nanostructured Na-ion and Li-ion anodes for battery application: a comparative overview. *Nano Res* 2017;10:3942-69. DOI
19. Zhou L, Zhang K, Hu Z, et al. Recent developments on and prospects for electrode materials with hierarchical structures for lithium-ion batteries. *Adv Energy Mater* 2018;8:1701415. DOI
20. Tiwari JN, Tiwari RN, Kim KS. Zero-dimensional, one-dimensional, two-dimensional and three-dimensional nanostructured materials for advanced electrochemical energy devices. *Prog Mater Sci* 2012;57:724-803. DOI
21. Cui H, Guo Y, Ma W, Zhou Z. 2D materials for electrochemical energy storage: design, preparation, and application. *ChemSusChem* 2020;13:1155-71. DOI
22. Chen R, Zhao T, Zhang X, Li L, Wu F. Advanced cathode materials for lithium-ion batteries using nanoarchitectonics. *Nanoscale Horiz* 2016;1:423-44. DOI
23. Liang J, Kou H, Ding S. Complex hollow bowl-like nanostructures: synthesis, application, and perspective. *Adv Funct Mater* 2021;31:2007801. DOI
24. Mei J, Wang T, Qi D, et al. Three-dimensional fast Na-ion transport in sodium titanate nanoarchitectures via engineering of oxygen vacancies and bismuth substitution. *ACS Nano* 2021;15:13604-15. DOI
25. Yu L, Hu H, Wu HB, Lou XW. Complex hollow nanostructures: synthesis and energy-related applications. *Adv Mater* 2017;29:1604563. DOI PubMed
26. Jiang J, Nie G, Nie P, et al. Nanohollow carbon for rechargeable batteries: ongoing progresses and challenges. *Nanomicro Lett* 2020;12:183. DOI PubMed PMC
27. Xie F, Zhang L, Ye C, Jaroniec M, Qiao SZ. The application of hollow structured anodes for sodium-ion batteries: from simple to complex systems. *Adv Mater* 2019;31:e1800492. DOI
28. Wu C, Tong X, Ai Y, et al. A review: enhanced anodes of Li/Na-ion batteries based on yolk-shell structured nanomaterials. *Nanomicro Lett* 2018;10:40. DOI PubMed PMC
29. Lu W, Guo X, Luo Y, Li Q, Zhu R, Pang H. Core-shell materials for advanced batteries. *Chem Eng J* 2019;355:208-37. DOI
30. Su L, Jing Y, Zhou Z. Li ion battery materials with core-shell nanostructures. *Nanoscale* 2011;3:3967-83. DOI
31. Wei Q, Xiong F, Tan S, et al. Porous one-dimensional nanomaterials: design, fabrication and applications in electrochemical energy storage. *Adv Mater* 2017;29:1602300. DOI
32. Tian W, Zhang H, Duan X, Sun H, Shao G, Wang S. Porous carbons: structure-oriented design and versatile applications. *Adv Funct Mater* 2020;30:1909265. DOI
33. Li J, Cao C, Xu X, Zhu Y, Yao R. $LiNi_{1/3}Co_{1/3}Mn_{1/3}O_2$ hollow nano-micro hierarchical microspheres with enhanced performances as

cathodes for lithium-ion batteries. *J Mater Chem A* 2013;1:11848-52. DOI

34. Zhu Z, Wang S, Du J, et al. Ultrasmall Sn nanoparticles embedded in nitrogen-doped porous carbon as high-performance anode for lithium-ion batteries. *Nano Lett* 2014;14:153-7. DOI
35. Zhang M, Li Y, Wu F, Bai Y, Wu C. Boost sodium-ion batteries to commercialization: strategies to enhance initial coulombic efficiency of hard carbon anode. *Nano Energy* 2021;82:105738. DOI
36. Liu Y, Merinov BV, Goddard WA 3rd. Origin of low sodium capacity in graphite and generally weak substrate binding of Na and Mg among alkali and alkaline earth metals. *Proc Natl Acad Sci USA* 2016;113:3735-9. DOI PubMed PMC
37. Dong R, Zheng L, Bai Y, et al. Elucidating the mechanism of fast Na storage kinetics in ether electrolytes for hard carbon anodes. *Adv Mater* 2021;33:e2008810. DOI
38. Dong R, Wu F, Bai Y, et al. Tailoring defects in hard carbon anode towards enhanced Na storage performance. *Energy Mater Adv* 2022;2022:9896218. DOI
39. Ge P. Electrochemical intercalation of sodium in graphite. *Solid State Ion* 1988;28-30:1172-5. DOI
40. Jache B, Adelhelm P. Use of graphite as a highly reversible electrode with superior cycle life for sodium-ion batteries by making use of co-intercalation phenomena. *Angew Chem Int Ed* 2014;53:10169-73. DOI PubMed
41. Stevens DA, Dahn JR. High capacity anode materials for rechargeable sodium-ion batteries. *J Electrochem Soc* 2000;147:1271-3. DOI
42. Wu F, Liu L, Yuan Y, et al. Expanding interlayer spacing of hard carbon by natural K^+ doping to boost Na-ion storage. *ACS Appl Mater Interfaces* 2018;10:27030-8. DOI
43. Yu K, Zhao H, Wang X, et al. Hyperaccumulation route to Ca-rich hard carbon materials with cation self-incorporation and interlayer spacing optimization for high-performance sodium-ion batteries. *ACS Appl Mater Interfaces* 2020;12:10544-53. DOI
44. Wu F, Zhang M, Bai Y, Wang X, Dong R, Wu C. Lotus seedpod-derived hard carbon with hierarchical porous structure as stable anode for sodium-ion batteries. *ACS Appl Mater Interfaces* 2019;11:12554-61. DOI
45. Yu K, Wang X, Yang H, Bai Y, Wu C. Insight to defects regulation on sugarcane waste-derived hard carbon anode for sodium-ion batteries. *J Energy Chem* 2021;55:499-508. DOI
46. Wang N, Chu C, Xu X, et al. Comprehensive new insights and perspectives into Ti-based anodes for next-generation alkaline metal (Na^+, K^+) ion batteries. *Adv Energy Mater* 2018;8:1801888. DOI
47. Dong S, Lv N, Wu Y, Zhang Y, Zhu G, Dong X. Titanates for sodium-ion storage. *Nano Today* 2022;42:101349. DOI
48. Ni Q, Dong R, Bai Y, et al. Superior sodium-storage behavior of flexible anatase TiO_2 promoted by oxygen vacancies. *Energy Stor Mater* 2020;25:903-11. DOI
49. Li Y, Zhang R, Qian J, et al. Construct NiSe/NiO heterostructures on NiSe anode to induce fast kinetics for sodium-ion batteries. *Energy Mater Adv* 2023;4:0044. DOI
50. Li Y, Wu F, Qian J, et al. Metal chalcogenides with heterostructures for high-performance rechargeable batteries. *Small Science* 2021;1:2100012. DOI
51. Li Y, Xu Y, Wang Z, et al. Stable carbon-selenium bonds for enhanced performance in *Tremella* -like 2D chalcogenide battery anode. *Adv Energy Mater* 2018;8:1800927. DOI
52. Li Y, Qian J, Zhang M, et al. Co-construction of sulfur vacancies and heterojunctions in tungsten disulfide to induce fast electronic/ionic diffusion kinetics for sodium-ion batteries. *Adv Mater* 2020;32:e2005802. DOI
53. Xiao Y, Lee SH, Sun YK. The application of metal sulfides in sodium ion batteries. *Adv Energy Mater* 2017;7:1601329. DOI
54. Klein F, Jache B, Bhide A, Adelhelm P. Conversion reactions for sodium-ion batteries. *Phys Chem Chem Phys* 2013;15:15876-87. DOI PubMed
55. Tan H, Chen D, Rui X, Yu Y. Peering into alloy anodes for sodium-ion batteries: current trends, challenges, and opportunities. *Adv Funct Mater* 2019;29:1808745. DOI
56. Li Y, Yuan Y, Bai Y, et al. Insights into the Na^+ storage mechanism of phosphorus-functionalized hard carbon as ultrahigh capacity anodes. *Adv Energy Mater* 2018;8:1702781. DOI
57. Fukunishi M, Yabuuchi N, Dahbi M, et al. Impact of the cut-off voltage on cyclability and passive interphase of Sn-polyacrylate composite electrodes for sodium-ion batteries. *J Phys Chem C* 2016;120:15017-26. DOI
58. Xiao X, Li X, Zheng S, Shao J, Xue H, Pang H. Nanostructured germanium anode materials for advanced rechargeable batteries. *Adv Mater Inter* 2017;4:1600798. DOI
59. Darwiche A, Marino C, Sougrati MT, Fraisse B, Stievano L, Monconduit L. Better cycling performances of bulk Sb in Na-ion batteries compared to Li-ion systems: an unexpected electrochemical mechanism. *J Am Chem Soc* 2012;134:20805-11. DOI PubMed
60. Su D, Dou S, Wang G. Bismuth: a new anode for the Na-ion battery. *Nano Energy* 2015;12:88-95. DOI
61. Marbella LE, Evans ML, Groh MF, et al. Sodiation and desodiation via helical phosphorus intermediates in high-capacity anodes for sodium-ion batteries. *J Am Chem Soc* 2018;140:7994-8004. DOI
62. Jung SC, Jung DS, Choi JW, Han YK. Atom-level understanding of the sodiation process in silicon anode material. *J Phys Chem Lett* 2014;5:1283-8. DOI PubMed
63. Zhu N, Zhang K, Wu F, Bai Y, Wu C. Ionic liquid-based electrolytes for aluminum/magnesium/sodium-ion batteries. *Energy Mater Adv* 2021;2021:9204217. DOI
64. Baughman RH, Shacklette LW, Murthy NS, Miller GG, Elsenbaumer RL. The evolution of structure during the alkali metal doping of

polyacetylene and poly(p-phenylene). *Mol Cryst Liq Cryst* 1985;118:253-61. DOI

65. Desai AV, Morris RE, Armstrong AR. Advances in organic anode materials for Na-/K-ion rechargeable batteries. *ChemSusChem* 2020;13:4866-84. DOI PubMed PMC
66. Tang K, Fu L, White RJ, et al. Hollow carbon nanospheres with superior rate capability for sodium-based batteries. *Adv Energy Mater* 2012;2:873-7. DOI
67. Gong Y, Yu C, Li Y, Qian J, Wu C, Bai Y. Constructing robust solid electrolyte interface via ZrO_2 coating layer for hard carbon anode in sodium-ion batteries. *Batteries* 2022;8:115. DOI
68. Chen X, Fang Y, Lu H, et al. Microstructure-dependent charge/discharge behaviors of hollow carbon spheres and its implication for sodium storage mechanism on hard carbon anodes. *Small* 2021;17:e2102248. DOI
69. Han H, Chen X, Qian J, et al. Hollow carbon nanofibers as high-performance anode materials for sodium-ion batteries. *Nanoscale* 2019;11:21999-2005. DOI
70. Zhong S, Liu H, Wei D, et al. Long-aspect-ratio N-rich carbon nanotubes as anode material for sodium and lithium ion batteries. *Chem Eng J* 2020;395:125054. DOI
71. Jia H, Dirican M, Sun N, et al. SnS hollow nanofibers as anode materials for sodium-ion batteries with high capacity and ultra-long cycling stability. *Chem Commun* 2019;55:505-8. DOI
72. Hou Z, Zhang X, Chen J, Qian Y, Chen L, Lee PS. Towards high-performance aqueous sodium ion batteries: constructing hollow $NaTi_2(PO_4)_3$@C nanocube anode with Zn metal-induced pre-sodiation and deep eutectic electrolyte. *Adv Energy Mater* 2022;12:2104053. DOI
73. Zhang Y, Wang P, Yin Y, et al. Heterostructured SnS-ZnS@C hollow nanoboxes embedded in graphene for high performance lithium and sodium ion batteries. *Chem Eng J* 2019;356:1042-51. DOI
74. Liu Z, Yu XY, Lou XW, Paik U. Sb@C coaxial nanotubes as a superior long-life and high-rate anode for sodium ion batteries. *Energy Environ Sci* 2016;9:2314-8. DOI
75. Bin DS, Li Y, Sun YG, et al. Structural engineering of multishelled hollow carbon nanostructures for high-performance Na-ion battery anode. *Adv Energy Mater* 2018;8:1800855. DOI
76. Wang X, Chen Y, Fang Y, Zhang J, Gao S, Lou XWD. Synthesis of cobalt sulfide multi-shelled nanoboxes with precisely controlled two to five shells for sodium-ion batteries. *Angew Chem Int Ed* 2019;58:2675-9. DOI
77. Yang D, Zhang S, Yu P, et al. Structure engineering of vanadium tetrasulfides for high-capacity and high-rate sodium storage. *Small* 2022;18:e2107058. DOI
78. Xie F, Zhang L, Su D, Jaroniec M, Qiao SZ. $Na_2Ti_3O_7$@N-doped carbon hollow spheres for sodium-ion batteries with excellent rate performance. *Adv Mater* 2017;29:1700989. DOI PubMed
79. Ru J, He T, Chen B, et al. Covalent assembly of MoS_2 nanosheets with SnS nanodots as linkages for lithium/sodium-ion batteries. *Angew Chem Int Ed* 2020;59:14621-7. DOI
80. Osman S, Peng C, Shen J, et al. Boosting fast and stable symmetric sodium-ion storage by synergistic engineering and amorphous structure. *Nano Energy* 2022;100:107481. DOI
81. Pan Q, Tong Z, Su Y, Qin S, Tang Y. Energy storage mechanism, challenge and design strategies of metal sulfides for rechargeable sodium/potassium-ion batteries. *Adv Funct Mater* 2021;31:2103912. DOI
82. Zhu J, Wei P, Zeng Q, et al. MnS@N,S co-doped carbon core/shell nanocubes: sulfur-bridged bonds enhanced Na-storage properties revealed by in situ raman spectroscopy and transmission electron microscopy. *Small* 2020;16:e2003001. DOI
83. Lim H, Yu S, Choi W, Kim SO. Hierarchically designed nitrogen-doped MoS_2/silicon oxycarbide nanoscale heterostructure as high-performance sodium-ion battery anode. *ACS Nano* 2021;15:7409-20. DOI PubMed
84. Zhang S, Qiu L, Zheng Y, et al. Rational design of core-shell ZnTe@N-doped carbon nanowires for high gravimetric and volumetric alkali metal ion storage. *Adv Funct Mater* 2021;31:2006425. DOI
85. Shen Y, Li Y, Deng S, et al. TiC/C core/shell nanowires arrays as advanced anode of sodium ion batteries. *Chin Chem Lett* 2020;31:846-50. DOI
86. Liu Y, Xu Y, Zhu Y, et al. Tin-coated viral nanoforests as sodium-ion battery anodes. *ACS Nano* 2013;7:3627-34. DOI
87. Li R, Zhang G, Zhang P, et al. Accelerating ion transport via in-situ formation of built-in electric field for fast charging sodium-ion batteries. *Chem Eng J* 2022;450:138019. DOI
88. Yang H, Xu R, Yao Y, Ye S, Zhou X, Yu Y. Multicore-shell Bi@N-doped carbon nanospheres for high power density and long cycle life sodium- and potassium-ion anodes. *Adv Funct Mater* 2019;29:1809195. DOI
89. Huang Y, Hu X, Li J, et al. Rational construction of heterostructured core-shell Bi_2S_3@Co_9S_8 complex hollow particles toward high-performance Li- and Na-ion storage. *Energy Stor Mater* 2020;29:121-30. DOI
90. Xie X, Huang K, Wu X, et al. Binding hierarchical $MoSe_2$ on MOF-derived N-doped carbon dodecahedron for fast and durable sodium-ion storage. *Carbon* 2020;169:1-8. DOI
91. Wang H, Xu D, Jia G, et al. Integration of flexibility, cyclability and high-capacity into one electrode for sodium-ion hybrid capacitors with low self-discharge rate. *Energy Stor Mater* 2020;25:114-23. DOI
92. Wang YX, Yang J, Chou SL, et al. Uniform yolk-shell iron sulfide-carbon nanospheres for superior sodium-iron sulfide batteries. *Nat Commun* 2015;6:8689. DOI PubMed PMC
93. Sun Q, Li D, Dai L, Liang Z, Ci L. Structural engineering of SnS_2 encapsulated in carbon nanoboxes for high-performance sodium/potassium-ion batteries anodes. *Small* 2020;16:e2005023. DOI PubMed

94. Xiao S, Li Z, Liu J, et al. Se-C bonding promoting fast and durable Na^+ storage in yolk-shell $SnSe_2$@Se-C. *Small* 2020;16:e2002486. DOI
95. Li Y, Zhang S, Wang S, et al. A multi-shelled V_2O_3/C composite with an overall coupled carbon scaffold enabling ultrafast and stable lithium/sodium storage. *J Mater Chem A* 2019;7:19234-40. DOI
96. Liu J, Kopold P, Wu C, van Aken PA, Maier J, Yu Y. Uniform yolk-shell Sn_4P_3@C nanospheres as high-capacity and cycle-stable anode materials for sodium-ion batteries. *Energy Environ Sci* 2015;8:3531-8. DOI
97. Qian J, Xiong Y, Cao Y, Ai X, Yang H. Synergistic Na-storage reactions in Sn_4P_3 as a high-capacity, cycle-stable anode of Na-ion batteries. *Nano Lett* 2014;14:1865-9. DOI PubMed
98. Yang H, Chen LW, He F, et al. Optimizing the void size of yolk-shell Bi@Void@C nanospheres for high-power-density sodium-ion batteries. *Nano Lett* 2020;20:758-67. DOI
99. Chen S, Huang S, Zhang YF, et al. Constructing stress-release layer on Fe_7Se_8-based composite for highly stable sodium-storage. *Nano Energy* 2020;69:104389. DOI
100. Zou F, Chen YM, Liu K, et al. Metal organic frameworks derived hierarchical hollow NiO/Ni/graphene composites for lithium and sodium storage. *ACS Nano* 2016;10:377-86. DOI
101. Liang H, Ni J, Li L. Bio-inspired engineering of Bi_2S_3-PPy yolk-shell composite for highly durable lithium and sodium storage. *Nano Energy* 2017;33:213-20. DOI
102. Feng X, Li Y, Zhang M, et al. Sulfur encapsulation and sulfur doping synergistically enhance sodium ion storage in microporous carbon anodes. *ACS Appl Mater Interfaces* 2022;14:50992-1000. DOI
103. Ni D, Sun W, Wang Z, et al. Heteroatom-doped mesoporous hollow carbon spheres for fast sodium storage with an ultralong cycle life. *Adv Energy Mater* 2019;9:1900036. DOI
104. Yang C, Li W, Yang Z, Gu L, Yu Y. Nanoconfined antimony in sulfur and nitrogen co-doped three-dimensionally (3D) interconnected macroporous carbon for high-performance sodium-ion batteries. *Nano Energy* 2015;18:12-9. DOI
105. Bai J, Zhang L, Li S, Ren H, Liu Y, Guo S. Self-assembled $MoTe_2$ hierarchical nanoflowers with carbon coating as anode material for excellent sodium storage performance. *Chem Eng J* 2023;452:139111. DOI
106. Opra DP, Neumoin AI, Sinebryukhov SL, et al. Moss-like hierarchical architecture self-assembled by ultrathin $Na_2Ti_3O_7$ nanotubes: synthesis, electrical conductivity, and electrochemical performance in sodium-ion batteries. *Nanomaterials* 2022;12:1905. DOI PubMed PMC
107. Li S, Wang Z, Liu J, et al. Yolk-shell Sn@C eggette-like nanostructure: application in lithium-ion and sodium-ion batteries. *ACS Appl Mater Interfaces* 2016;8:19438-45. DOI